Received: 7 September 2021 | Revised: 18 November 2021 | Accepted: 20 November 2021

DOI: 10.1002/aoc.6537

RESEARCH ARTICLE

Applied Organometallic Chemistry WILEY

Some characteristics of new and innovative COX inhibitor derivatives: Potent hCA-I and hCA-II inhibitors supported by molecular docking studies

Emel Karakılıç[1] | Zuhal Alım[2] | Mustafa Emirik[3] | Arif Baran[1]

[1]Department of Chemistry, Faculty of Science and Arts, Sakarya University, Sakarya, Turkey

[2]Department of Chemistry, Faculty of Science and Arts, Kırşehir Ahi Evran University, Kırşehir, Turkey

[3]Department of Chemistry, Faculty of Science and Arts, RecepTayyip Erdoğan University, Rize, Turkey

Correspondence
Arif Baran, Department of Chemistry, Sakarya University, 54187, Sakarya, Turkey.
Email: abaran@sakarya.edu.tr

Funding information
Scientific and Technological Research Council of Turkey (TÜBITAK), Grant/Award Numbers: 115Z446, 217Z043

Abstract

In this study, two novel metallophthalocyanines (ZnPc and CoPc) were synthesized using the corresponding metal salts 4-(4-(4-[4-chlorophenyl]-5-methylisoxazol-3-yl)phenoxy)-phthalonitrile (**11**), prepared from the reaction of 4-nitrophthalonitrile and 4-(4-[4-chlorophenyl]-5-methylisoxazol-3-yl)phenol (**9**). These metallophthalocyanines (MPcs) showed quite solubility in organic solvents such as dichloromethane (DCM), tetrahydrofuran (THF), dimethyl formamide (DMF), and dimethylsulfoxide (DMSO). The novel compounds **11a** and **11b** have been characterized using their UV–Vis, FT–IR, ^{1}H NMR, ^{13}C NMR, X-Ray, and MALDI–TOF mass spectra. Supporting information cocerning with the study has been supplied. Photochemical, photophysical, and cyclic voltagram properties of these novel 4-(4-(4-[4-chlorophenyl]-5-methylisoxazol-3-yl)phenoxy substituted metallophthalocyanines (**11a** and **11b**) were determined in DMF. DNA binding, metal chelating effect assay, and DPPH [2,2-diphenyl-1-picrylhydrazyl hydrate] radical scavenging assay and electrochemical studies of MPcs were investigated. Further, the inhibitory effects of the COX-inhibitor based novel metallophthalocyanines (**11a** and **11b**) and their ligands (**10** and **11**) were examined on human erythrocyte carbonic anhydrase I (hCA-I) and II (hCA-II) isoenzymes, and the synthesized molecules exhibited very strong inhibitory effects on both isoforms. In addition, the hCA-I and hCA-II inhibition potential of Zn (II) and Co (II) Phthalocyanine complexes was supported by molecular docking studies. The binding interaction of metallophthalocyanines complexes **11a**, **11b** enzymes were analyzed in detail.

KEYWORDS

DNA-binding, enzyme, inhibitors, metal complexes, molecular docking

1 | INTRODUCTION

Phthalocyanines (Pcs) are stable molecules against heat, light and solvents. Due to the these properties, they have been used for many years in different fields such as electrical conductivity, optical storage devices,[1] gas sensors, antioxidant potential, dyes, and pigments,[2,3] photovoltaic optics,[4–6] solar cells,[7–9] laser dyes,[10,11] chemical sensors,[12–15] nonlinear optics,[16,17] semiconductors,[18–20] liquid crystals,[21] catalytic activity, electrochromic properties, and paint industries.[22,23] Also, phthalocyanines are used as an alternative treatment and diagnostic technique for cancer, and are used as photosensitizers in PDT by stimulating electrons from molecular oxygen transferred to reactive single oxygen species (ROS) in tissue.[24,25] It is very important to use photosensitizers in the removal of tumor tissues without the need for surgical intervention. While radiotherapy, chemotherapy and surgery may have some side effects such as organ dysfunction occur in the body, in PDT treatment there is no side effects like this.[26–28] The another important factor that makes phthalocyanines viable depends on their solubility. For example; the solubility in common solvents is low, closing the solution path for the fabrication of electronic and photonic devices.[29] However, this adverse effect can be eliminated by adding appropriate solubility enhancing side groups. Azoles, using as appropriate solubility enhancing side groups, are compounds in the pharmaceutical industry that have numerous applications and are critical for the synthesis of complex molecules. In particular, five member aromatic heterocyclic isoxazols; muscimol (**1**) has been used as a GABAA agonist and a psychotropic drug,[30] ibotenic acid (**2**) used as a neurotoxin,[31] leflunomide (**3**) used as an immuno suppressive agent effective in the treatment of rheumatoid arthritis,[32] isocarboxazid (**4**) used as an antidepresant and oxidase inhibitors (MAOIs),[33] cycloserine (**5**) used as in multidrug-resistant tuberculosis (MDR-TB) treatment,[34] parecoxib and valdecoxib (**6**) used as a COX-II selective inhibitors,[35–38] 5-aminoisoxazoles and 5-alkylisoxazoles used in the construction of molecules with antihistaminic, analgesic, antibacterial, insecticidal, antiviral activity (Figure 1).[39]

The determination of dual inhibitors of human carbonic anhydrase and human cyclooxygenase enzymes for the development of new generation drugs, especially for use in cancer treatment, is an interesting topic with promising future in the field of medicinal chemistry.[40,41] So, the selective oxygenase inhibitor derivatives were treated against carbonic anhydrate isoforms-I and -II, which had a strong inhibitory effect on the CA inhibitor isoforms. There are two main groups of CA inhibitor isoforms (isoform I and isoform II). The first isoform is the inorganic anions that make the metal complex; the second isoform is the molecules containing the sulfonamide group. Considering these two groups, various pharmacological classes of CA inhibitors have been developed.[42] Selective COX-2 inhibitors containing the sulfonamide group also act as potent inhibitors of various CA isoenzymes.[41,43] For example, it has been determined that palmacoxib,[44] celecoxib,[45] valdecoxib,[46] which are selective inhibitors of COX-2, also have a strong inhibitory effect on CA-I and CA-II isoenzymes.

Based on this result, the researchers stated that the potential side effects of COX-2 inhibitors could be reduced by the inhibitory effect of COX-2 inhibitors on CAI and CAII isoenzymes[44] Therefore, studies to determine the effect of COX inhibitors on CA-I and CA-II. isoenzymes are very important in terms of evaluating the potential clinical effectiveness of these inhibitors.

In this study, the synthesis, characterization, determination of photochemical properties and inhibition effects on human erythrocytes hCA-I and hCA-II izoenzymes of new and novelty COX-inhibitor based metallophthalocyanines containing substituted azole groups were aimed. For this purpose, synthesis, purification and characterization of ZnPc (**11a**) and CoPc (**11b**) metallophthalocyanine compounds, which interdependent with 4-(4-(4-[4-chlorophenyl]-5-methylisoxazol-3-yl)phenoxy)-phthalonitrile (**11**) units, were conducted. Then, DNA binding, metal chelating effect assay, and DPPH [2,2-diphenyl-1-picrylhydrazyl hydrate] radical scavenging assay and electrochemical studies of these

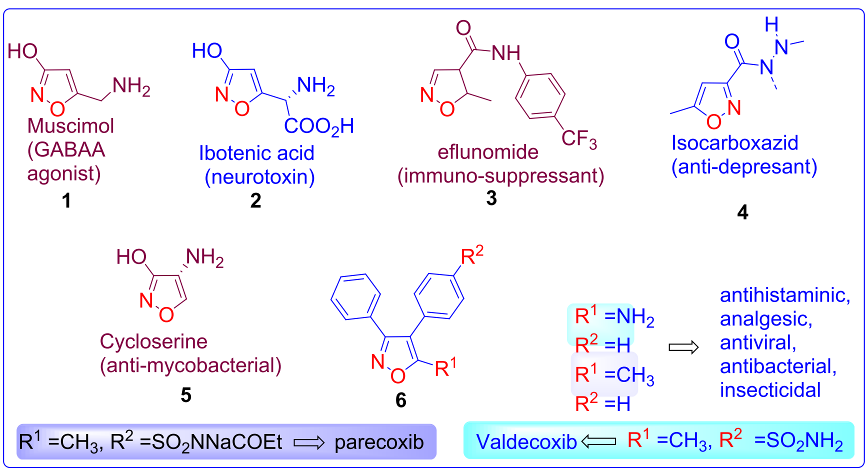

FIGURE 1 Selected examples of isoxazoles with pharmacological activity

molecules were investigated. And also the inhibition effects of these molecules on hCA-I and hCA-II isoenzymes were examined. We believe that the results obtained in the study will make a significant contribution to the literature.

2 | EXPERIMENTAL

2.1 | Materials and chemicals

4-Hydroxybenzaldehyde, bezylchloride, hydroxyamoniumchloride, pyridine, N-chlorosuksinimide (NCS), hydrochloric acid (HCl), 4-chlorophenylacetone, sodium hydride (NaH), triethylamin (TEA), 4-nitrophthalonitrile, potassium carbonate (K_2CO_3), 1,8-diazabicyclo[5.4.0]undec-7-ene (DBU), Zn $(OAc)_2.2H_2O$, Co $(OAc)_2.4H_2O$, 1,3-diphenylisobenzofuran (DPBF), 4-nitrophenyl acetate (Sigma), potassium phosphate buffer, calf thymus DNA (CT-DNA) (Sigma), uric acid, tetrabutylammonium hexafluorophosphate ($TBAPF_6$) were obtained from commercial suppliers. The solvents such as acetone, tetrahydrofuran (THF), diethylether, dimethyl sulfoxide (DMSO), dichloromethane (DCM), N, N-Dimethylformamide (DMF), and ethanol were dried and purified.

2.2 | Equipment

^{1}H NMR and ^{13}C NMR spectra were recorded in $CDCl_3$ (d 7.26 and 77.0 for ^{1}H and ^{13}C NMR, respectively) using an VARIAN Infinity Plus 300 MHz NMR spectrometer with and TMS as the internal standards. UV–Vis spectra was measured on a Shimadzu UV 2600 model spectrophotometer and Infrared spectra were recorded on an Ati Unicam Mattson 1000 Series FT–IR (ATR system) spectrometer. MALDI–TOF spectra were recorded on Bruker Daltonics flex Analysis. Fluorescence spectra were measured in a quartz cuvette using Hitachi U-2910 and Fluoro Max-4 (Horiba Jobin Yvon), respectively. Elemental analysis was carried out by a LECO 932 CHNS-O apparatus. General Electric a light source a halogen lamp (500 W) was used. A 550-nm glass cut off filter (schott) and a water filter off infrared radiation and ultraviolet, respectively.

2.3 | Synthesis

For the synthesis of compound (**9**); the cycloaddition reaction of arylnitriloxide (**8**) and 4-chlorophenylacetone (**7**) was carried out as in literatures.[38,47,48]

2.3.1 | Synthesis of 4-(4-[4-chlorophenyl]-5-methylisoxazol-3-yl)phenol (10)

The synthesis of compound **10** was prepared as in the literature with little modification.[49] To a solution of compound **9** (1.0 g, 2.66 mmol) and Pd/C (10%, 0.18 g) in ethyl acetate (100 ml) was stirred at room temperature under H_2 atmosphere. The completion of the reaction was followed by TLC indication, finished after for 18 h. After the filtration of the solution the filtrate was concentrated to give **10** as a colorless residue, recrystallization of the residue gave white crystals (0.7 g, 93%). Mp 178–180°C. FT–IR max cm^{-1}: 3161 cm^{-1} (–OH); 1611, 1594, 1471 cm^{-1} (C=N, C=C); 1230, 1173, 1091 (C-O and C-N). ^{1}H NMR (300 MHz, DMSO-d_6) δ 9.85 (s, 1H, OH), 7.44 (d, $J = 8.5$ Hz, AA′ part of AA′BB′ system 2H, H_a and H_a'), 7.19 (d, $J = 8.5$ Hz, BB′ part of AA′BB′ system, 2H, H_b and H_b'), 7.13 (d, $J = 8.6$ Hz, AA′ part of AA′BB′ system, 2H, H_c and H_c'), 6.74 (d, $J = 8.6$ Hz, BB′ part of AA′BB′ system, 2H, H_d and H_d'), 2.48 (s, 3H, [-CH_3]); ^{13}C NMR (75 MHz, DMSO-d_6) δ; 167.4, 161.0, 159.4, 133.1, 132.1 (2C), 130.2, 129.6 (2C), 129.5 (2C), 119.6, 116.2 (2C), 114.5, 12.0.

2.3.2 | Synthesis of 4-(4-(4-[4-chlorophenyl]-5-methylisoxazol-3-yl)phenoxy)phthalonitrile (11)

4-nitrophthalonitrile (0.61 g, 3.50 mmol) and 4-(4-[4-chlorophenyl]-5-methylisoxazol-3-yl)phenol **10** (1.0 g, 3.50 mmol) was dissolved in 25 mL of DMF. K_2CO_3 was added over the mixture for 15 min intervals and the mixture was stirred at 50°C for 24 h under N_2 atmosphere. The reaction was stopped and then precipitated in ice water. It was filtered, washed with plenty of water and then dried. A white solid product was obtained. Yield; 1.1 g (76%). Mp 161–163°C. FT–IR max cm^{-1}: 3089 cm^{-1} (Ar–H); 2929 cm^{-1} (aliphatic C–H); 2234 cm^{-1} (C ≡ N); 1629, 1592, 1564 cm^{-1} (C=N, C=C); 1247, 1209, 1012 (C-O and C-N). ^{1}H NMR (300 MHz, $CDCl_3$) δ 7.67 (d, $J = 8.4$ Hz, 1H), 7.44 (d, $J = 8.2$ Hz, 2H), 7.32 (d, $J = 7.9$ Hz, 2H), 7.24 (s, 1H), 7.19 (d, $J = 8.2$ Hz, 1H), 7.06 (d, $J = 7.9$ Hz, 2H), 6.96 (d, $J = 7.9$ Hz, 2H), 2.38 (s, 3H); ^{13}C NMR (75 MHz, $CDCl_3$) δ; 167.5, 161.3, 160.0, 154.9, 135.8, 134.3, 131.3, 130.9, 129.5, 128.7, 127.1, 122.3, 122.1, 120.8, 118.0, 115.1, 115.0, 109.7, 11.8.

2.3.3 | Synthesis of zinc (II) phthalocyanine (11a)

Compound **11** (0.2 g, 0.48 mmol) and Zn $(OAc)_2.2H_2O$ (0.05 g, 0.24 mmol) dissolved in 15 ml of DMF. 2–3 drops of DBU were added onto the solution. The reaction was then stirred for 24 h at 130°C under $N_{2(g)}$ atmosphere. The progression of the reaction was controlled with TLC in THF and MeOH, 1/1 ratio. The mixture was precipitated in 100 ml of ice water. The precipitate was filtered, washed with hot water and hot alcohol, and dried. 0.10 g of dark green solid product was obtained. This compound is readily soluble DCM, THF, DMF and DMSO. Yield; 48%. Mp > 350°C. FT–IR max cm^{-1}: 2956 cm^{-1} (Ar–H); 2925, 2855 cm^{-1} (aliphatic C–H); 1601, 1519, 1492 cm^{-1} (C=N, C=C); 1229, 1168, 1090, 1012 (C-O and C-N). UV–Vis (DMF), λ_{max}, nm: 679, 612, 358. MALDI–TOF MS: m/z $[M]^+$ calcd. For $C_{96}H_{56}Cl_4N_{12}O_8Zn$:1711.76; found $[M + H]^+$ 1712.87.

2.3.4 | Synthesis of cobalt (II) phthalocyanine (11b)

Compound **11** (0.2 g, 0.48 mmol) and Co $(OAc)_2.4H_2O$ (0.06 g, 0.24 mmol) dissolved in 15 mL of DMF. 2–3 drops of DBU were added onto the solution. The reaction was then stirred for 24 h at 130°C under $N_{2(g)}$ atmosphere. The mixture was precipitated in 100 ml of ice water. The precipitate was filtered, washed with hot water and hot alcohol, and dried. 0.12 g of dark green solid product was obtained. This compound is readily soluble DCM, THF, DMF and DMSO. Yield; 63%. Mp > 350°C. FT–IR ν_{max} (cm^{-1}): 2952, 2925 cm^{-1} (Ar–H); 2855 cm^{-1} (aliphatic C–H); 1601, 1519, 1491 cm^{-1} (C=N, C=C); 1232, 1167, 1012 (C-O and C-N). UV–vis (DMF), λ_{max}, nm: 666, 600, 331. MALDI-TOF MS: m/z $[M]^+$ calcd. For $C_{96}H_{56}Cl_4N_{12}O_8Co$:1705.31; found $[M + H]^+$ 1707.39.

2.4 | X-ray data collection of compound (11)

Crystal Dimensions: Compound **11**, approximate 0.13 x 0.12 x 0.10 mm was mounted on a glass fiber. *Crystal System*: triclinic, *Lattice Type*: Primitive, *Lattice Parameters*: a = 8.7996 (12) Å, b = 9.7400 (11) Å, c = 12.7902 (16) Å, α = 86.169 (5)°, β = 82.076 (6)°, γ = 67.850 (5)°, V = 1005.5 (2) $Å^3$, *Space Group*: P-1, *Z value*: 2, *Dcalc*: 1.360 g cm^{-3}, *F000*: 424, *μ (MoKα)*: 0.22 mm^{-1}. *Diffractometer*: Measurements were made on a BRUKER D8-QUEST diffractometer with graphite monochromated, *Radiation*: MoKα (λ = 0.71070 Å), *Absorption correction*: multi-scan, *Detector Position*: distance was 40.00 mm, *θmax/θmin*: 26.4°/2.5°, *No. of Reflections Measured*: Total: 33893, Unique: 4111 (Rint = 0.076), *Absorption*: T_{min} = 0.678, T_{max} = 0.745. Structure Solution: Direct Methods, Refinement: Full-matrix least-squares on F2, Anomalous Dispersion: All non-hydrogen atoms, No. Observations (I > 2.00σ[I]): 2566, $R[F^2 > 2\sigma(F^2)]$: 0.057, $wR(F^2)$: 0.160, Goodness of Fit Indicator: 1.04, Maximum peak in Final Diff. Map: 0.24 e−/$Å^3$, Minimum peak in Final Diff. Map: −0.43 e−/$Å^3$.

The structure solution and refinement were realized by direct methods using SHELXS-97 and refined by full-matrix least squares methods on F^2 using SHELXL-97,[50] All non-hydrogen atoms were refined with anisotropic parameters. All H atoms were located from difference maps and then treated as riding atoms with C-H distances of 0.93–0.98 Å. The following procedures were implemented in our analysis: program used for molecular graphics were as follow: MERCURY program,[51] software used to prepare material for publication: WinGX[52] Supramolecular analyses were made and the diagrams were prepared with the aid of PLATON.[53]

2.5 | Electrochemical study

In this study, cyclic voltammograms of ZnPc and CoPc compounds (Dyes) were recorded on Gamry Interphase 1000 potentiostat with their electrode system; glassy carbon as working electrode, Pt disk as reference electrode, Pt wire as counter electrode at a scan rate of 100 mV s^{-1}. All electrochemical measurements were carried out in DMF solvent containing tetrabutylammonium hexafluorophosphate ($TBAPF_6$) as supporting electrode and Fc/Fc + redox couple was utilized as external standard to calibrate the results.

2.6 | Enzyme inhibition studies

2.6.1 | Isolation and purification of carbonic anhydrase hCA-I and hCA-II izoforms

Isoenzymes I and II were purified from human erythrocytes using the sepharose-4B-L-tyrosine sulfanilamide affinity column at 280 nm as in our previous studies.[54–56] The activities of isoenzymes were measured as in Wilbur–Anderson,[57] purification and quantitative protein determination was done as in Bradford method.[58] The purity of The hCA-I and hCA-II isoenzymes was checked by Laemmli's SDS-PAGE method (3%–8%),[59] imaged as a single protein band at approximately 29 kDa. Active enzyme fractions were pooled and dialyzed overnight against 0.05 M $Tris\text{-}SO_4$ (pH 7.4) buffer. After dialysis, hCA-I and hCA-II isoenzymes were separated into small fractions of 1 ml before storation at

−80°C for using. During the experimental studies, carbonic anhydrase use the *p*-nitrophenyl acetate as substrate and hydrolyzes *p*-nitrophenyl acetate to *p*-nitrophenol and acetic acid. The formation of *p*-nitrophenol from *p*-nitrophenyl acetate is monitored by measuring the absorbance at 348 nm, 25°C for 3 min using a spectrophotometer. The enzyme unit was calculated using the absorption coefficient ($\varepsilon = 5.4 \times 10^3\ M^{-1}\ cm^{-1}$) of *p*-nitrophenyl acetate at 348 nm.[60] The enzyme unit is defined as the amount of enzyme that hydrolyzes one micromole of *p*-nitrophenyl acetate to *p*-nitrophenol and acetic acid under optimal conditions at 25°C.

2.6.2 | In vitro inhibition studies on hCA-I and hCA-II izoenzymes

After isolation and purification of enzyme izoforms, the inhibitory effects of the COX-inhibitor based novel metallophthalocyanines (**11a** and **11b**) and their ligands (**10** and **11**) were determined on the esterase activity of hCA-I and hCA-II. The activities were assayed in the presence of at least five different concentrations of inhibitors. The experiments were repeated in triplicate for each inhibitor concentration. The control activity of the enzyme was accepted as 100%, and activity % plots against the inhibitor concentration were plotted. From these graphs, IC_{50} values expressing the inhibitor concentration that reduced the enzyme's activity by half were determined. Acetazolamide (AZA) used as a standard inhibitor for hCA-I and hCA-II isoenzymes.

2.7 | Moleculer docking assay

2.7.1 | Target preparation

Crystal structure of human Carbonic anhydrase-I (hCA-I) and Crystal structure of human carbonic anhydrase isozyme II (hCA-II) were selected for docking studies with pdb id: 5GMM and 3 M98, respectively.[61,62] X-ray crystal structures of hCA-I and hCA-II were downloaded from PDB Databank (www.rcsb.org/) with resolutions 2.0 Å and 1.5 Å, respectively. Enzyme structures were prepared using the Maestro Protein Preparation Wizard.[63] During preparation, the missing side chains were filled using the Prime Module and water molecules except within 5 Å from the bound ligand were removed. The OPLS-2005 force field was applied to minimize the structure of the protein. The PROPKA module of Maestro was used to define the protonation states of amino acid residues. Schrodinger Suite software was used for these procedures.[64]

2.7.2 | Ligand preparation

The 3D-Structures of reference ligand, acetazolamide (Aza) and polmacoxib (Pox) were obtained from the PubChem database (https://pubchem.ncbi.nlm.nih.gov/). 3-D structures of the metallophthalocyanine complexes (**11a** and **11b**) and metal free ligand **10** and **11** were drawn in gauss view GUI. The most stable conformers of entire ligands were obtained by using Gaussian 09 software employing the semiempirical PM6 method in the implicit solvent of water with the CPCM method. The best conformers were further optimized by the DFT/wB97XD/6–31 G(d,p) level. The optimized structures were exposed to ligand preparation procedure on the LigPrep module to produce the possible 3D conformations under the neutral pH by using the OPLS3 force field and saved in the sdf file format.

2.7.3 | Docking protocol

The AutoDock Vina-based CB-Dock server was used for the docking experiments.[65] CB-Dock automatically predicts binding regions of a given protein, calculates the centers and sizes with a curvature-based cavity detection approach, customizes the docking box size, and then performs molecular docking with AutoDock Vina.[66] Autodock Vina use both genetic and local search, a hybrid Lamarckian genetic algorithm.[67] The results of docking calculations were evaluated as Vina scores. The docked pose with the best Vina score and cavity size was selected to analyze the binding mode using the Maestro pose viewer. Five different binding sites for each ligand were defined as the target grid center and set to the default value of 9 as the pose required for the completion of each insertion. Vina scores were used as Gibbs free binding energies obtained from each run. The best binding free energies obtained for each region were also used for the calculation of Boltzmann-averaged binding energies (ΔG_{ba}) by means of the Boltzmann distribution equation (Equation 1), where the number 5 represents each binding region of enzyme.[68] ΔG_{ba} were utilized to calculate binding constants using the following Equation 1: $K_b = \exp[-\Delta G_{ba}/RT]$, where R is the gas constant and $T = 298$ K.

$$\Delta G_{ba} = \sum_{i=1}^{5} \frac{e^{-\Delta G_i/kT}}{\sum_{i=1}^{5} e^{-\Delta G_i/kT}} \Delta G_i \qquad (1)$$

3 | RESULTS AND DISCUSSION

3.1 | Chemistry

In this study, the cyclooxygenase (COX) enzyme inhibitors, catalyzes the speed limiting phase in the prostanoids formation from arachidonic acid (AA). Oxygenase inhibitors encoded by two different genes are known as COX-1 and COX-2 isoforms. COX-1, known as the cleaning gene, is present in all tissues, and while high COX-1 expression is present in thrombocyte and gastric mucosa, COX-2 responds to inflammatory and mitogenic stimuli.[38] Therefore synthesis and biological studies of new active molecules by placing oxygenase enzyme inhibitors such as compound **10**, in a different skeleton are important. The synthesis was initiated by 1,3-dipolar cycloaddition. It is think that the aryl nitrile oxides **8** are considered to be a good precursor for 1,3-dipolar cycloaddition to achieved the synthesis of oxygenase inhibitor derivative **9** by using cycloaddition reaction of arylnitrile oxides **8** to the phenylacetone enolate ion **7** regioselectively in the presence of lithium diisopropylamide at 0°C afforded **9** (yield 65%)[38,47,48] debenzylation reaction of compound **9** with Pd/C (10%) in ethyl acetate at room temperature under H_2 atmosphere was afforded compound **10** (Scheme 1).[69] The cyclooxygenase derivative **10** was turned to ftalonitrile compound **11** in DMF using 4-nitrophthalonitrile. After, the metallophthalocyanines compounds **11a** and **11b** were performed, their characterization, photophysical, photochemical and electrochemical properties were performed, and also this metallophthalocyanines and their ligands (**10** and **11**) were evaluated on the esterase activity of hCA-I and hCA-II against acetazolamide (AZA).

i. NaH, THF, 0°C, **ii.** EtOH, Pd/C 10%, H_2, 25°C, **iii.** EtOH, Pd/C 10%, H_2, 25°C, **iv.** 4-Nitrophthalonitrile, K_2CO_3, DMF, 50°C, 24 h. in quant.

Thus, oxygenase inhibitor derivative **10** was reacted with 4-nitrophthalonitrile in DMF in the presence of potassium carbonate to obtain new phthalonitrile compound **11** (Scheme 1).[69] Phthalonitrile compound **11** is thought to have the advantage of application studies for N4-macrocyclic core of ZnPc and CoPc as ligand. Therefore, the structure of this compound was studied in detail. In the ^{1}H-NMR spectrum of compound **11**, symmetric protons resonated in the deserved region, giving doublets for the two phenyl groups attached to the isooxazole ring. Three other prominent protons for the nitrile bonded ring resonated at 7.67 ppm as doublet 7.67 ($J = 8.4$ Hz, 1H), 7.24 ppm as singlet (s, 1H) and 7.19 ppm as doublet ($J = 8.2$ Hz, 1H), respectively. The 20 lines in the ^{13}C-NMR spectra also confirm the structure. IR spectra of phthalonitrile compounds exhibited the aromatic (Ar-H) peak at 3089 cm^{-1} the aliphatic (Ar-H) peak at 2929 cm^{-1}; the most prominent nitrile (C$\equiv$N) peak at 2234 cm^{-1}; the double bond (C$=$C, N$=$N) peak at 1629, 1592, 1564 cm^{-1}; the single bond (C-O, C-N) peak at 1247, 1209, 1012 cm^{-1}. For the further analysis, the single crystal structure analysis of compound **11** was performed (Figure 2).

In this study, peripheral tetra-substituted compounds containing new Zn (II) phthalocyanine (ZnPc) **11a** and cobalt (II) phthalocyanine (CoPc) **11b** were synthesized. In the procedure, after the ligand **11** and Zn $(OAc)_2.2H_2O$ or Co $(OAc)_2.4H_2O$ were dissolved in DMF, then DBU

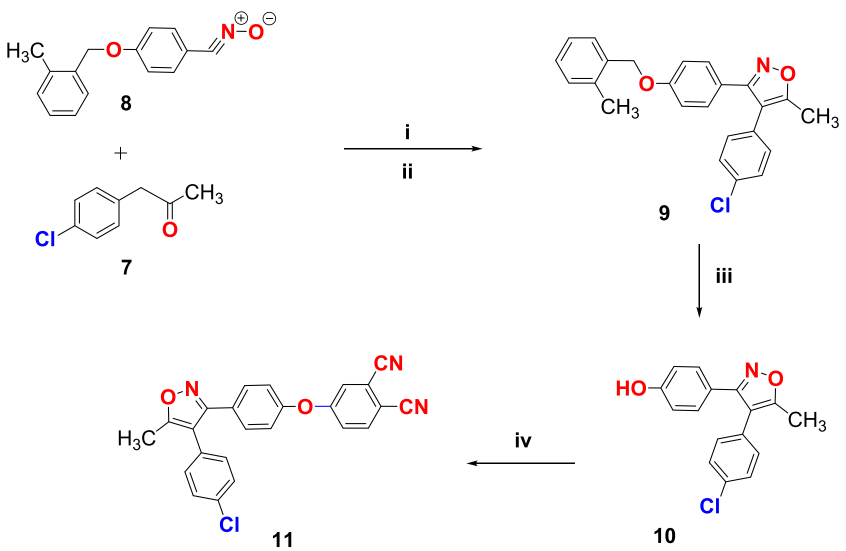

i. NaH, THF, 0ºC, **ii.** EtOH, Pd/C 10%, H_2, 25 ºC, **iii.** EtOH, Pd/C 10%, H_2, 25 ºC, **iv.** 4-Nitrophthalonitrile, K_2CO_3, DMF, 50 ºC, 24h. in quant.

SCHEME 1 Synthesis route of compounds **9**, **10**, and **11**

FIGURE 2 Crystal structures of **11**

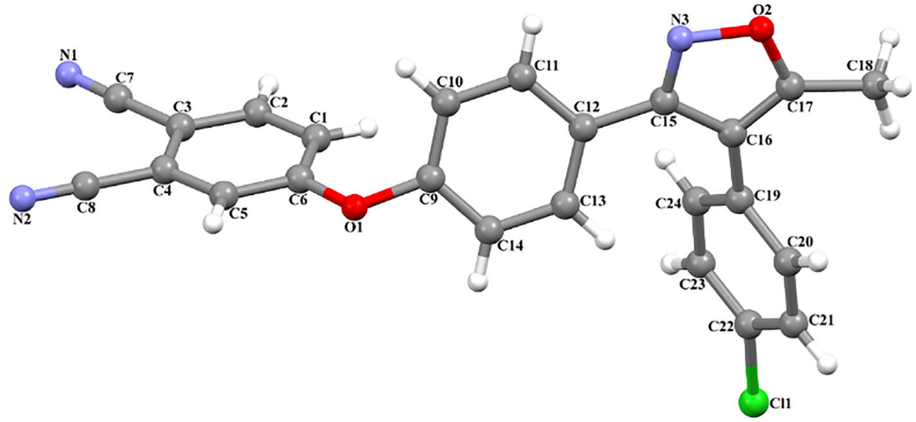

SCHEME 2 Synthetic route of compounds **11a**, and **11b** from ligand **11**

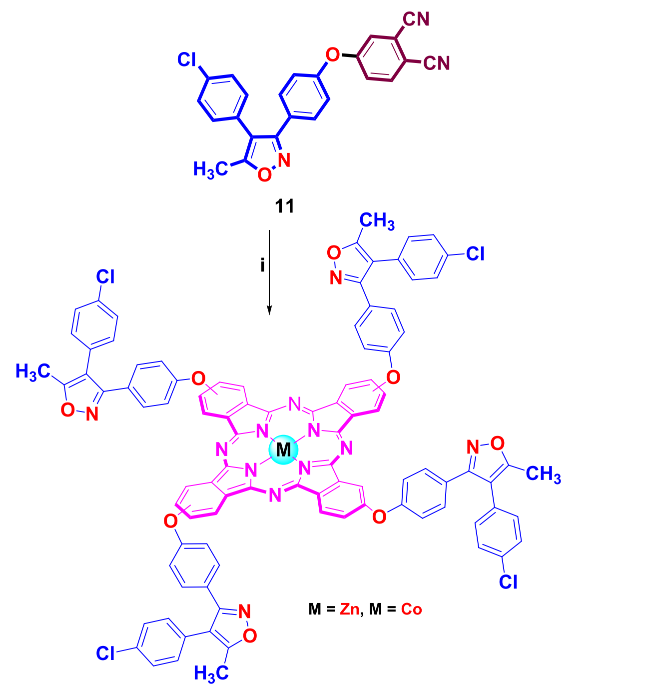

i. 11a Zn(OAc)$_2$.2H$_2$O, DMF, DBU(1-3 drop), 130 °C, 24 h, (48%), **11b** Co(OAc)$_2$.4H$_2$O, DMF, DBU(1-3 drop), 130 °C, 24 h, (63%)

(2–3 drops) were added onto the stirred solution under the $N_{2(g)}$ atmosphere at reflux temperature. The progression of the reaction was controlled with TLC in THF and MeOH, 1/1 ratio. The forming phthalocyanines after 24 h were participated and washed with water then hot ethanol resulted in 48% yield for ZnPc and 63% yield for CoPc respectively (Scheme 2).

3.2 | Synthesis and characterization

The synthetic procedure for the new compounds is outlined in Scheme 2. **11a** and **11b** phthalocyanine compounds demonstrated good solubility in organic solvents such as THF, DCM, Chloroform ($CHCl_3$), DMF and DMSO. The novel compounds **11a** and **11b** have been characterized using their FT–IR, MALDI–TOF, and UV–Vis. The analysis of **11a** was characterized by IR spectra exhibiting aromatic (Ar-H) peak 2956 cm^{-1}; aliphatic (C-H) peaks at 2925, 2855 cm^{-1}; (C=N, C=C) peaks at 1601, 1519, 1492 cm^{-1}; (C-O and C-N) peaks at 1229, 1168, 1090, 1012 cm^{-1}. Likewise, the compound **11b** exhibited aromatic (Ar-H) peaks 2952; aliphatic (C-H) peaks at 2925 cm^{-1}, 2855 cm^{-1}; (C=N, C=C) peaks at 1601, 1519, 1491 cm^{-1}; (C-O and C-N) peaks at 1232, 1167, 1012 cm^{-1} in IR spectra. Also, the absence of the nitrile (C ≡ N) peak at 2234 cm^{-1} indicates the formation of compounds **11a** and **11b**. The molecular ion peak for the mass spectra of phthalocyanines **11a** and **11b** were also documented. This ion peaks gave m/z

[M] + calcd. For **11a** ($C_{96}H_{56}C_{14}N_{12}O_8Zn$):1711.76; found [M + H] + 1712.87 and for **11b** ($C_{96}H_{56}C_{14}N_{12}O_8Co$):1705.31; found [M + H] + 1707.39. The MALDI–TOF MS results were found to be consistent with the proposed structures.

3.3 | Crystal structure of compound 11

The molecular structure of compound **11** with the atom labeling is shown in Figure 2. Both nitriles in molecule are equivalent and typical of N ≡ C triple bonds [1.137 (3) and 1.140 (3) Å]. The C6-O1-C9 bond angle is 119.45 (19)°, while the C12-C15-C16-C19 torsion angle is 5.4(4)°. The dihedral angles between isoxazole and phenyl rings are 23.11 (15)° and 55.67 (12)°. The molecules of compound **11** are connected by C-H⋯N hydrogen bonds. The C10 atom acts as hydrogen-bond donor, via atom H10, to atom N_2 in the molecule at ($-x$, $1 - y$, $-z$), forming a centrosymmetric $R_2^2(18)$ ring centered at (0, 1/2, 0). The compound **11** also contains three C-H⋯π interactions. The combination of these interactions produces 3D framework.

3.4 | UV–Vis absorption and aggregation studies

In phthalocyanines is very important to determine the two absorption bands (B and Q bands) by UV–Vis. One of these absorption bands is the B band in the visible region at rougly 300–450 nm, and the other is the Q band in the visible region at 600–750 nm for metallophthalocyanines. It is seen that absorptions belonging to B band transition from low energy π levels to LUMO, whereas the Q-band is bonded to the $\pi \rightarrow \pi^*$ transition from the highest occupied molecular orbital (HOMO) to the lowest unoccupied molecular orbital (LUMO) of the phthalocyanine ring.

UV–Vis spectrophotometer of ZnPc (**11a**) and CoPc (**11b**) phthalocyanine complexes were taken in different solvents at a concentration of 1×10^{-5} M. Aggregation behavior of Pc is defined as the coplanar association of rings from monomer to dimer. The aggregation behavior varies depending on the concentration, solvent, structure of the substituents, metal ions, and temperature.[70] When aggregation occurs as a result of intramolecular interactions between the Pc units of MPcs, the electronic absorption spectrum of the Q band at the 630- to 645-nm region is observed.[71] It is seen that these compounds make long wavelength shift (red shift) in Q band position in DCM. The compounds **11a** and **11b** were not aggregated in DMF, DMSO and THF, but they were slightly agglomerated at 618 nm (for **11a**) and 616 nm (for **11b**) in DCM (Figure 3a,b).

In addition, the absorption of prepared phthalocyanine compounds (**11a** and **11b**) in DMF at concentration range of 12×10^{-6} and 2×10^{-6} was measured and aggregation properties were investigated (Figure 4a,b, respectively). As the concentration increased, it was not observed that compounds **11a** and **11b** shifted any wavelength (blue or red). In addition, concentration of these compounds against the absorbance graph was plotted and it was found to comply with Lambert–Beer law.

3.5 | Photochemical parameters

3.5.1 | Singlet oxygen quantum yields (Φ_Δ)

Singlet oxygen is generated when its triplet state interacts with photosensitizer through a process called light sensitization. Ideal photosensitizers are known for their ability to produce phototoxic single oxygen.

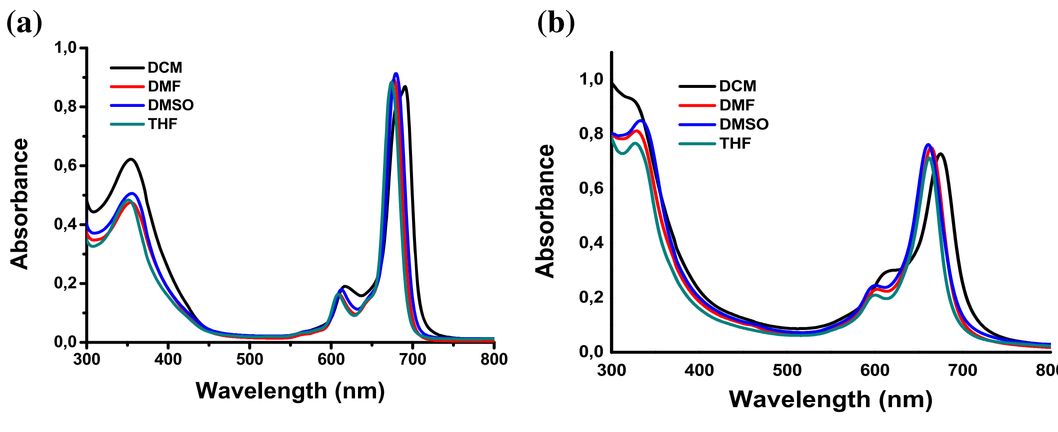

FIGURE 3 UV–Vis absorption spectra of (a) **11a** and (b) **11b** in different solutions. Concentration = 1.00×10^{-5} M

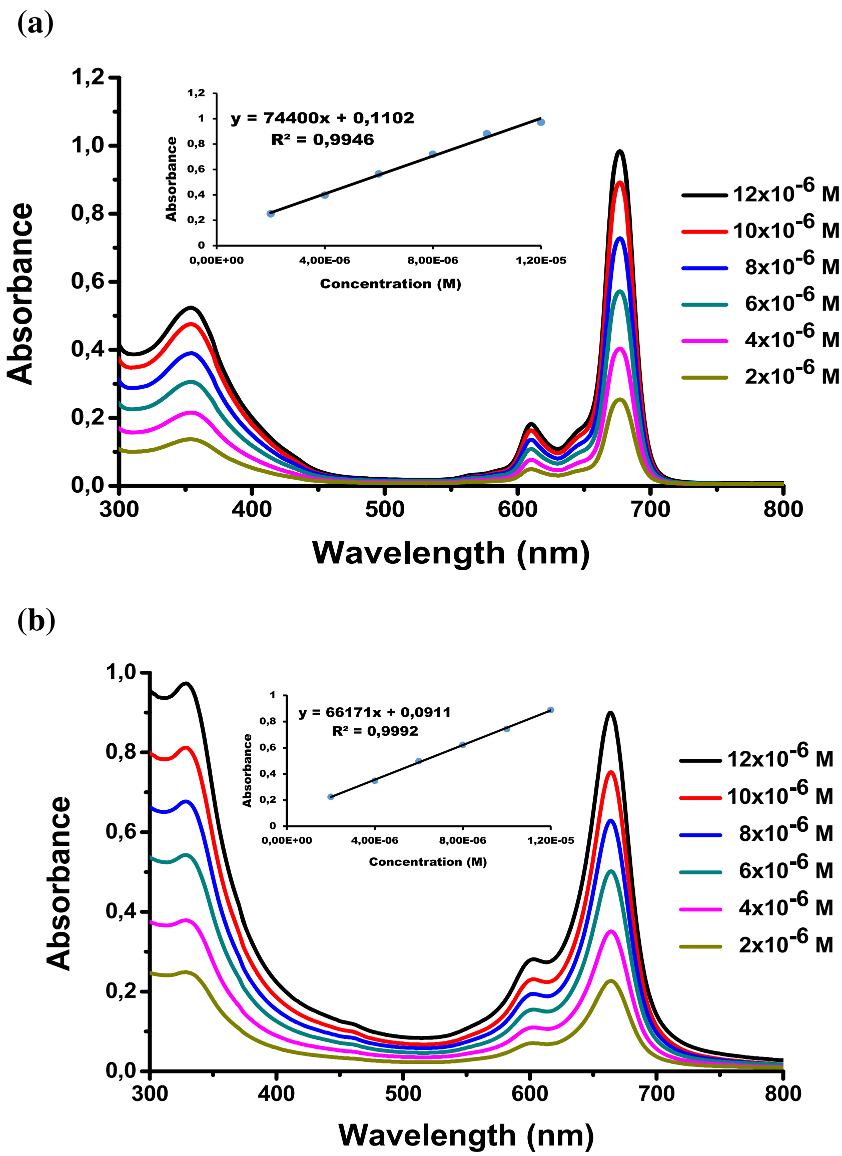

FIGURE 4 Absorbance changes of compound **11a** (a) and **11b** (b) in DMF at concentrations from 12×10^{-6} to 2×10^{-6} M

The amount of single oxygen formed after the stimulation of phthalocyanines is explained as single oxygen quantum yield (Φ_Δ).[72] When singlet oxygen generation has a low yield, it is possible to increase the yield by using various photosensitizers. Singlet oxygen quantum yield is defined as the ratio of the number of moles of theoretically occurring singlet oxygen to the number of moles of absorptive photons. However, in practice singlet oxygen is determined by consumption with the aid of an extinguisher.

To measure singlet oxygen quantum yield of compound **11a** at $1.0\text{x}10^{-5}$ M in DMF was performed according to the known method using singlet oxygen quencher *1,3-Diphenylisobenzofuran* (*DPBF*) at $1.0\text{x}10^{-3}$ M. The time-dependent decrease in absorbance of this quencher every 5 seconds was monitored spectroscopically using 8.15×10^{15} photon s^{-1} cm^{-2} light at 417 nm (Figure 5). Since the DPBF compound was very sensitive to light, the solution was prepared in the dark. Singlet oxygen quantum yield was calculated using Equation 2 (Table 1).

The singlet oxygen quantum yield is calculated by the following equation.

$$\Phi_\Delta = \Phi_\Delta^{Std} \frac{R\ .\ I_{abs}^{Std}}{R^{Std}.I_{abs}} \tag{2}$$

where $\boldsymbol{\Phi_\Delta^{Std}}$ is the singlet oxygen quantum yield ($\boldsymbol{\Phi_\Delta}$) for the standard Zn-Pc ($\boldsymbol{\Phi_\Delta^{Std}}$=0.56 in DMF)[74] $\boldsymbol{R}$ and $\boldsymbol{R^{Std}}$ are the DPBF photobleaching rates in the existence of the respective samples (**11a**) and standard. $\boldsymbol{I_{abs}}$ and $\boldsymbol{I_{abs}^{Std}}$ are the rates of light absorption by the samples (**11a**) and standard.

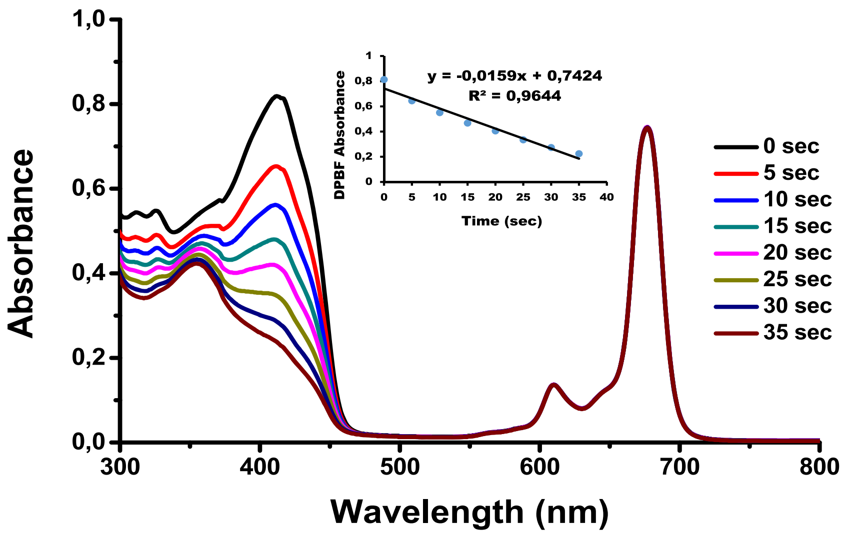

FIGURE 5 Absorbance changes for the determination of singlet oxygen quantum yield of complex **11a** (1.0×10^{-5} M) in DMF using DPBF as singlet oxygen quencher. (Inset: plot of DPBF absorbance versus time)

TABLE 1 Photochemical parameters of **11a** in DMF

Compound	Φ_Δ	Φ_d ($\times 10^{-4}$)
11a	0.44	0.26
ZnPc[a]	0.56	0.23

[a]Data from Zorlu et al.[73] and Baran et al.[74]

3.5.2 | Photodegradation quantum yield (Φ_d)

Photodegradation is the chemical reaction that results from exposure of molecules to light. As a result of these reactions may occur in chromophore groups. Chromophoric groups are special structures that can bind to color-imparting hydrocarbons. The calculation of the photodegradation quantum yield is made by examining the change in absorption spectrum during the photodegradation of the material. Photodegradation is detected by the change in the Q band. The synthesized compound **11a** was dissolved in DMF (1.0×10^{-5} M) and exposed to 3.26×10^{16} photons s^{-1} cm^{-2} light at certain time intervals and UV–vis spectra were taken to examine the change in Q bands at 679 nm. Accordingly, Figure 6 confirms that photo distortions without phototransformation occur with reduced Q-band density. According to Figure 6, photodisorders without phototransformation occur with a decrease in Q-band density. The Φ_d values of phthalocyanines are known to be as low as 10^{-6} for stable derivatives and 10^{-3} for unstable.[75] In addition, it is known that highly unstable molecules degrade before they have time to act, while highly stable molecules cannot be easily eliminated by the host organism.[73] According to the data in Table 1, it can be said that Zinc (II) phthalocyanine **11a** shows at close stability due to conjugation when compared to standard ZnPc.

Photodegradation quantum yield (Φ_d) is calculated by the following Equation 3.

$$\Phi_d = \frac{(C_0 - C_t).V.N_A}{I_{abs}.\ S.\ t} \tag{3}$$

where C_0 and Ct are the samples (**11a**) concentrations before and after irradiation, V is the reaction volume, N_A is the Avogadro's constant, S is the irradiated cell area, t is the irradiation time, and I_{abs} is the overlap integral of the radiation source light intensity and the absorption of the samples (**11a**).

3.6 | Fluorescence quenching studies 1,4-benzoquinone (BQ)

Fluorescence quenching properties of compound **11a** were performed using a saturated benzoquinone (BQ) solution at 1.0×10^{-5} M DMF. The results of quenching were found to be consistent with the kinetics of diffusion-controlled Bimolecular Reactions Kinetics (Stern-Volmer Kinetics). The fluorescence emission reduction of compound **11a** by the addition of BQ at different concentrations in DMF is shown in Figure 7.

Quinones are known to have high electron affinity and their participation in electron transfer processes is good.[76] The lowest stimulated state energy for Quinones is greater than the stimulated single state energy of MPc complexes.[77] Therefore, the transfer of energy from the stimulated MPc to the BQ is unlikely to take place; moreover, MPcs are known to decline easily. Fluorescence MPc quenching by BQ occurs by electron transfer from excited state from MPc to BQ.[78] Moreover, the Stern–Volmer constant (Ksv) value was found to be 68.4 M^{-1} on the slope plot plotted against BQ concentration. The

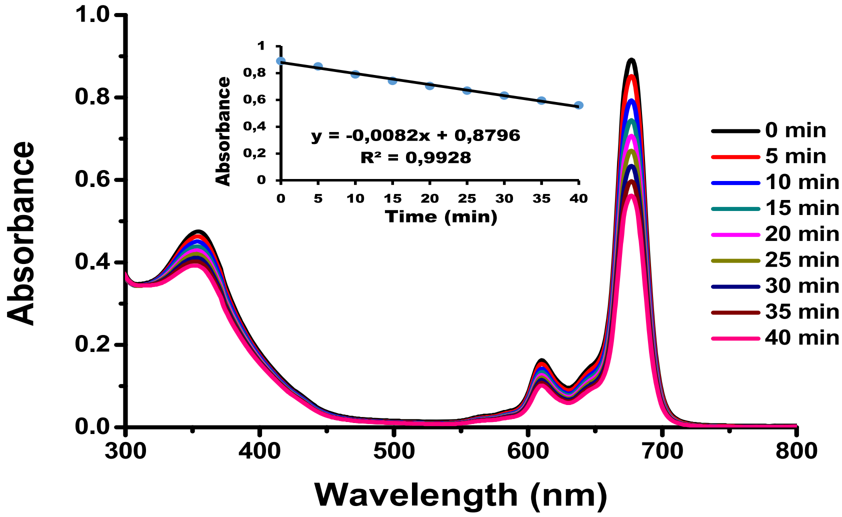

FIGURE 6 Electronic absorption spectral changes during the investigation of the photodegradation quantum yield of compound **11a** (1.0×10^{-5} M). (Inset: plot of absorbance versus time)

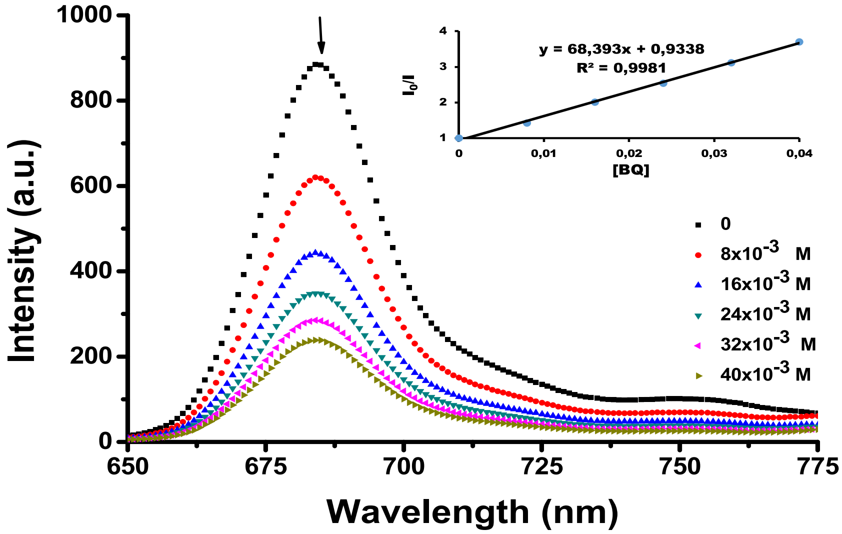

FIGURE 7 Flourescence emission spectral changes of **11a** (1.0×10^{-5} M) on addition of different concentrations of BQ in DMF. [BQ] = 0, 0.008, 0.016, 0.024, 0.032, 0.040 M

substituted complex **11a** appears to increase Ksv values in DMF with the Zn (II) complex group of continuous Schiff base containing continuous conjugation as compared to the standard ZnPc (Std-ZnPc = 57.60 M^{-1} in DMF).[73]

The changes in fluorescence emission spectra of substituted Zn (II) phthalocyanine **11a** by adding BQ in different concentration were studied. And also, the changes in fluorescence intensity related to BQ concentration by the Stern–Volmer (S–V) equation Equation 4 were recorded[79]:

$$I_0/I = 1 + K_{SV}[BQ]. \quad (4)$$

where I_0 and I are the fluorescence intensities of fluorophore in the absence and presence of quencher, respectively; [Q] is the concentration of the quencher, and Ksv is the Stern–Volmer constant.

3.7 | Electrochemical studies for ZnPc and CoPc compounds

Cyclic voltammetry (CV) was used to investigate the electrochemical properties of phtalocyanine compounds, **11a** and **11b**. (Figure 8).

Cyclic voltametry were utilized to investigate electrochemical properties for metal phythalocyanine complexes (MPc, M = Zn, Co). Cyclic voltamogrames of the complexes calibrated with external ferrocene standard (0,36 V vs. Pt disk pseudo-reference electrode) and recorded at 100 mV s^{-1} is given in Figure 8. Electrochemical parameters were tabulated at Table 2. MPcs showed an irrevesible oxidation at 0.70, 0.79 V and a reversible reduction peaks−1.12, −1.24 V for ZnPC and CoPc respectively, which can be assigned to ring based-redox processes.[80] An additional oxidation peak was appeared in CV of CoPc at 0.46 as cobalt is redox active matal

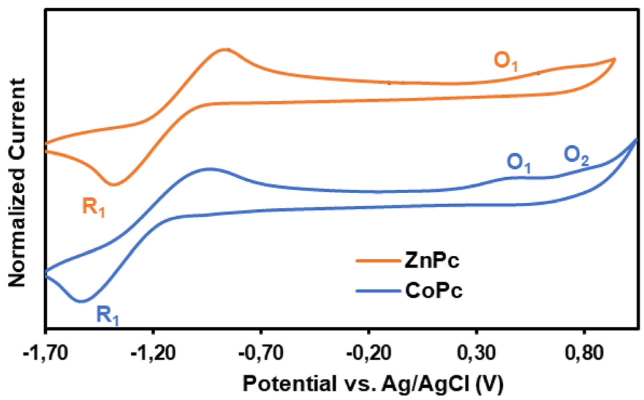

FIGURE 8 Cyclic voltammograms of **11a** and **11b** in DMF containing 0.1 M $TBABF_4$

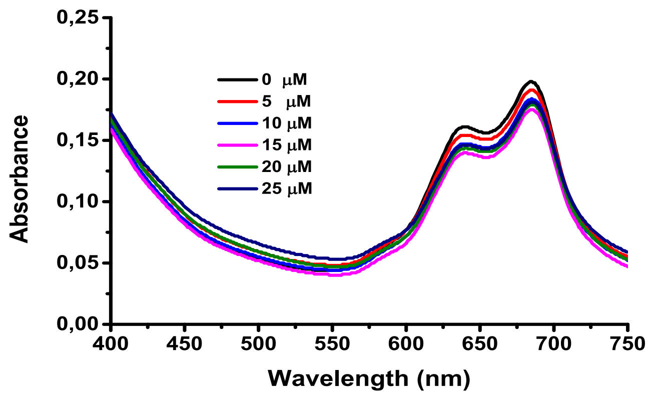

FIGURE 9 Absorption spectrum of **11a** upon increasing amounts of CT-DNA

TABLE 2 Electrochemical properties of **11a** and **11b**

Dye	λ_{max} (nm)	λ_{onset} (nm)	$E_{0\text{-}0}$ (eV)[a]	E_{red} (V)	E_{ox} (V)	E_{ox} (V)	$E_{HOMO/LUMO}$ (eV)[b,c]
11a	679	699	1.77	−1.12	0.70	—	−5.13/−3.36
11b	666	689	1.80	−1.24	0.79	0.46	−5.01/−3.21

[a]Band gap ($E_{0\text{-}0}$) was calculated from the absorption onset wavelength (λ_{onset}) using $E_{0\text{-}0} = 1240/\lambda_{onset}$.
[b]HOMO level was calculated by the equation HOMO $= -(4.8 + E_{1/2})$ (vs. Fc/Fc^+).[84] In this equation, 4.8 eV is the energy level of ferrocene/ferrocenium couple below the vacuum level.
[c]LUMO level was estimated from $E_{LUMO} = E_{HOMO} + E_{0\text{-}0}$.[85]

which results from the fact that central atom 3d orbitals of MPcs lie between HOMO and LUMO orbitals of the system at CoPcs but below the HOMO level of the system at ZnPcs.[81,82] CoPcs display blue shifted Q band maxima in the absorption spectra compared to ZnPc because the complexes bearing open-shell metal ions like cobalt (II) interact strongly with the Pc compared to zinc (II). This leads to lower absorption onset which corresponds to higher band gap energy.[83]

3.8 | Biological evaluation

3.8.1 | DNA binding studies

In the study of absorption spectra, predicting the DNA binding mode and the affinity of metal compounds with DNA is one of the important techniques. Experimental results show that metal phthalocyanine compounds bind to the DNA by intercalative binding mode, which has a high binding affinity for DNA.[86,87] Zinc phthalocyanine compound has been shown to interact with DNA and binding of the compound does not affect the structure of the phthalocyanine ring.[88] Electronic absorption titration is one of the most important techniques to estimate the binding mode and propensity of compounds by CT-DNA.[74] In electronic absorption titration, the strong interaction of π-π * between aromatic chromophore groups and DNA bases affects batchromism, hypochromicity and isosbestic point intercalation.[89] In the case of intercalation, a strong stacking interaction occurs between DNA base pairs and compounds. The strong stacking interaction, binding of an intercalative compound to DNA leads to hypochromism (reduced absorption intensity) and significant barochromism (red shift wavelength) in the absorption spectrum.[74]

In this study, titration with DNA in the absence and presence of CT-DNA was performed to investigate the binding mode of compounds **11a** and **11b** with DNA. However, compound **11b** did not bind to DNA because it produced aggregation in the aqueous solution, and also there was no red shift due to hypochromism and low binding constants. The compound **11a** gives a strong and characteristic Q-band absorption in the Q absorption region between 642 and 687 nm. The absorption spectrum of **11a** with increasing CT-DNA concentration is shown in Figure 9.

These results indicated that compound **11a** interacts with CT-DNA and binds to CT-DNA by intercalation binding mode, and accordingly, demonstrated 8.6% bathoromromic. The binding mode of compound **11a** with CT-DNA was analyzed quantitatively. K_b values of **11a** estimated from the Wolfe-Shimmer equation were $4.6 \times (\pm 0.56)\ 10^3\ M^{-1}$. The binding constant of **11a** is lower than the binding constant of ethidium bromide a known DNA intercalator ($K_b = 1.23 \pm 0.07 \times 10^5$). These results suggest the existence of non-intercalative interactions between synthesized phthalocyanines and CT-DNA.

3.8.2 | DPPH radical scavenging assay

1,1-diphenyl-2-picrylhydrazyl (DPPH) is widely used as free radical-scavenging in the determination of various free radical compounds. This process is based on the reduction of DPPH in the presence of an antioxidant in solution and the formation of non-radical DPPH-H by hydrogen-giving.[90] When the DPPH is reacted with the antioxidant compound that gives off a hydrogen atom, it causes the loss of violet color by reducing the antioxidant by giving it an H atom and forming the DPPH-H form.[91] The antioxidant properties of phthalocyanine compounds (**11a** and **11b**) were tested in vitro using DPPH free radical scavenging assay according to literature.[74] Radical scavenging activity results of Pc compounds compared to gallic acid are shown in Table 3. While **11a** showed weak DPPH radical scavenging capacity, **11b** showed better effect. (Study concentrations 6.65 ± 0.39%, 9.84 ± 0.42%, 23.66 ± 0.26%, 25.76 ± 0.39% and 10.2 ± 0.36%, 17.62 ± 0.31%, 23.25 ± 0.28%, 29.75 ± 0.41% **11a** and **11b**, respectively). **11a** and **11b** were not as effective as gallic acid when their DPPH radical scavenging capacities were taked into account (Figure 10).

3.8.3 | Metal chelating effects assay

Transition metals are essential elements that provide enzyme activity in the human body. But at the same time, unpaired electrons can react quickly with peroxides and form alkoxyl radicals. Therefore, chelating transition metals by antioxidants can be considered an important mechanism in the oxidation process.[92] In this study, metal chelating activities were determined by comparison with EDTA as reference compound. Experimental methods and applications were made according to literature.[74] Metal chelating activity of the phthalocyanines was determined at 25, 50, 75, and 100 μM concentrations using their 1 mM stock solutions in DMSO. Table 4 presents ferrous ions chelating activity (%) of **11a** and **11b**. For all studied samples the chalation activity increased while increasing their concentrations. **11a** and **11b** showed low ferrous ion chalation properties when compared with EDTA (Figure 11).

3.8.4 | In vitro inhibition results of COX-inhibitor based metallophthalocyanines on hCA-I and hCA-II izoenzymes

In the literature, it was reported that palmacoxib, celecoxib, valdecoxib'in had dual inhibitors effect on hCOX and hCA isoenzymes.[41,44–46] Also, in recent years, it has been determined that trimethyllithymide compounds and dihydrothiazole benzenesulfonamides have double inhibition effects for hCOX (COX1/COX2) isoenzymes and hCA (CAI/CAII/CAIX/CAXII) isoenzymes.[74]

Accordingly in this study, Zn (II) phthalocyanine (**11a**) and Co (II) phthalocyanine (**11b**) molecules were synthesized by placing the **10** molecule, which is a

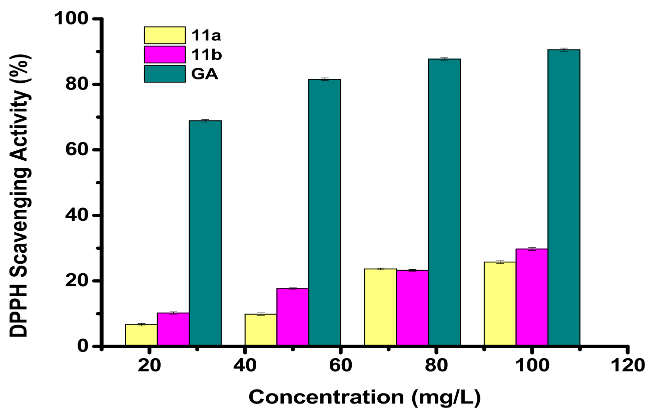

FIGURE 10 Radical-scavenging activity on DPPH radicals (%) of the **11a** and **11b** compounds. (GA: Gallic acid)

TABLE 3 Radical-scavenging activity on DPPH radicals (%) of the phthalocyanines

Concentrations (μM)[a]	11a	11b	Gallic acid[b]
25	6.65 ± 0.39[c]	10.2 ± 0.36[c]	68.88 ± 0.40[c]
50	9.84 ± 0.42[c]	17.62 ± 0.31[c]	81.53 ± 0.42[c]
75	23.66 ± 0.26[c]	23.25 ± 0.28[c]	87.71 ± 0.38[c]
100	25.76 ± 0.39[c]	29.75 ± 0.41[c]	90.58 ± 0.50[c]

[a]Four experiments were performed for all compounds in each experiment in triplicated.
[b]Reference compound.
[c]Mean values ± SD are shown for triplicate experiments.

TABLE 4 Ferrous ions chelating activity (%) of the phthalocyanines

Concentrations (μM)[a]	11a	11b	EDTA[b]
25	4.85 ± 0.20[c]	5.96 ± 0.22[c]	15.65 ± 0.15[c]
50	5.72 ± 0.32[c]	9.88 ± 0.29[c]	51.42 ± 0.18[b]
75	11.23 ± 0.19[c]	15.64 ± 0.22[b]	82.31 ± 0.08[c]
100	14.37 ± 0.23[c]	18.74 ± 0.29[c]	96.85 ± 0.21[c]

[a]Four experiments were performed for all compounds in each experiment in triplicate.
[b]Reference compound.
[c]Mean values ± SD are shown for triplicate experiments.

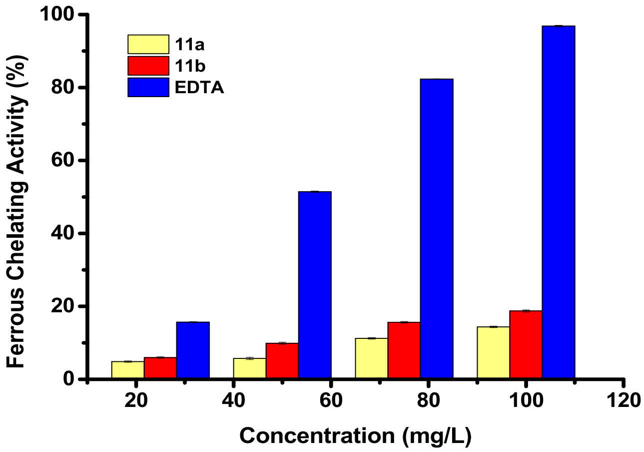

FIGURE 11 Chelating effect of **11a** and **11b** compounds on ferrous ion. (EDTA: Ethylenediaminetetraacetic acid)

cyclooxygenase enzyme inhibitor derivatives, in a different skeleton. The inhibitory effects of these COX-derivatives based metallophthalocyanines on hCA-I and hCA-II isoenzymes were investigated. IC_{50} values of **10**, **11**, **11a** and **11b** for hCA-I were found as 9.86 μM, 13.46 μM, 350 nM, 233 nM, respectively. Looking at these results, **11b** had a stronger inhibition effect than **11a** and its ligand **11** and **10** on hCA-I isoenyzme. A low IC_{50} value indicates a strong inhibitory effect. According to this, for hCA-I the order of the inhibitors is as follows: **11b** > **11a** > **10** > **11**. IC_{50} values of **10**, **11**, **11a** and **11b** for hCA-II were found as 11.86 μM, 14.76 μM, 350 nM, 233 nM, respectively. Also, For hCA-II the order of the inhibitors is as follows: **11b** > **11a** > **10** > **11**. According to the results, the inhibitory power of **11a** and **11b** molecules on hCA-I and hCA-II isoenzymes was found to be equal. It was seen that **11b** molecule containing Co (II) had a stronger inhibitory effect for both isoenzymes than **11a** containing Zn (II). In addition, **11a** and **11b** molecules were found to have a much stronger inhibitory effect than acetazolamide, which is the standard inhibitor of CA. On the other hand, ligands **10** and **11** had more effective inhibition for hCA-I than hCAII. IC_{50} graphs shown in Figure 12 and the inhibition results are summarized in Table 5. Also, in Figure 13, IC_{50} values of the **10**, **11**, **11a**, **11b** and AZA for hCA-I and hCA-II are given comparatively.

Consequently, when the results obtained in the experiment were compared with the AZA for hCA-I and hCA-II, we found that COX-inhibitor-based new metallophytolocyanines had an potent inhibitory effect on enzyme isoforms at nM levels. However, in these conditions, the inhibition of ligands on these enzyme isoforms was low even at μM levels. This is because the side chains and inner nuclei of the phthalocyanine ring with metal in their nuclei have a major impact on their inhibition abilities. When the metal enters the core, the metal chelating effect of phthalocyanines alters the electron density and facilitates the inhibitory activity.[93–95]

Also, it has been stated that by identifying dual inhibitors of hCOX and hCA isoenzymes, it is possible to reduce the side effects caused by COX inhibitors, especially to design higher-efficiency *anti*-cancer drugs in cancer treatment and emphasized that this is an important step for the design of dual inhibitors with common pharmacological properties.[41,44–46] Thus, we believe that our results will make a significant contribution to the literature on the design of hCOX and hCA dual inhibitors.

3.9 | Molecular docking studies

Docking studies were performed to investigate the inhibition potential of newly synthesized metallophthalocyanine complexes (MPc) and their free ligands against hCA-I and hCA-II. It was also used to define the interactions between the studied Pc complexes with the amino acid residues of the target proteins.

Based on the docking study, it was found that the ZnPc and CoPc were interacting with enzyme more strongly than the reference drug molecules and free ligands with range of Vina score −13.5 and −12.0 kcal mol^{-1}. The docking scores of each region and calculated ΔG_{ba} dependent binding constant of all studied compounds were given in Table 6. The results show

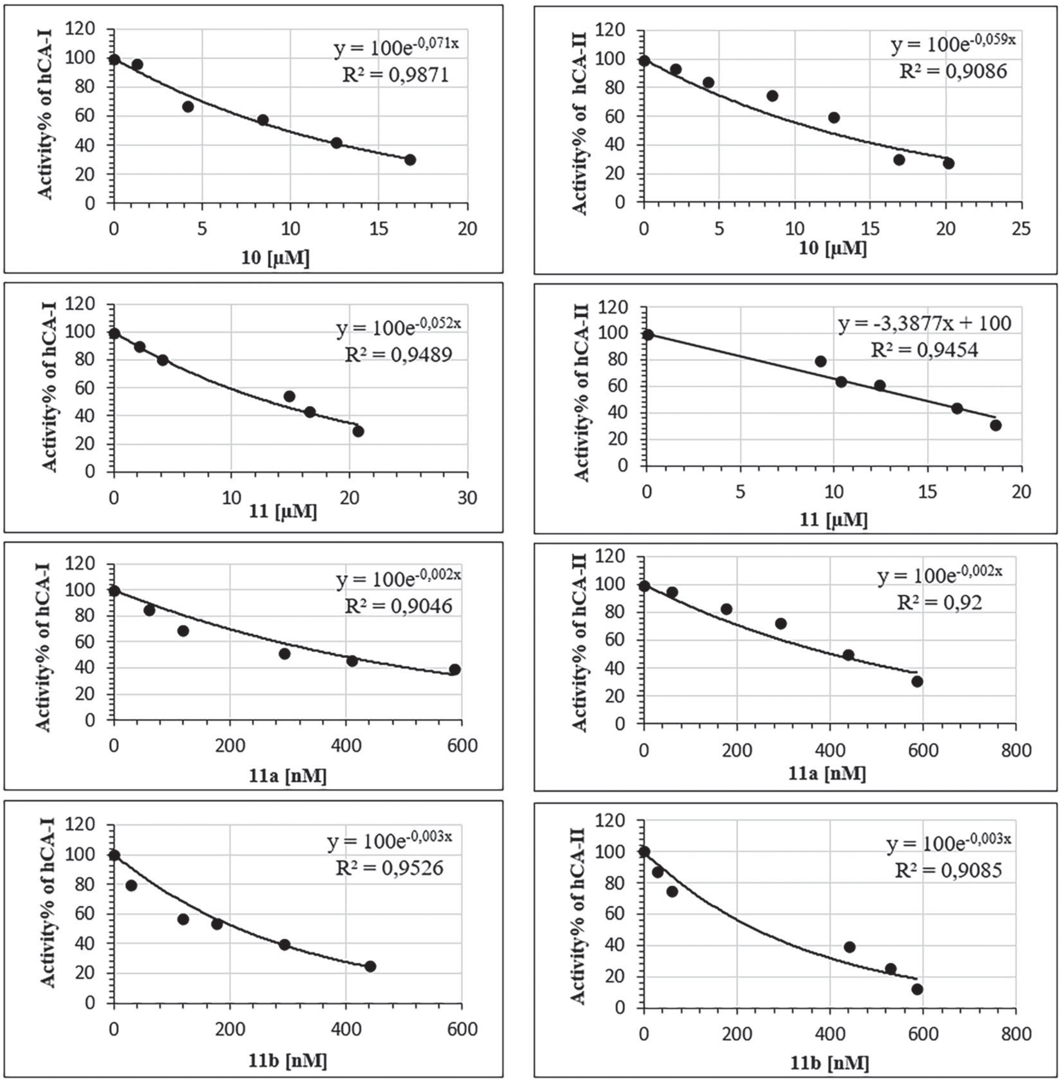

FIGURE 12 IC_{50} graphs of **10**, **11**, **11a**, **11b** for hCA-I and hCA-II izoenzymes

TABLE 5 Inhibition results of COX-inhibitor based metallophthalocyanines on hCA-I and hCA-II izoenzymes

Compounds	for hCA-I		for hCA-II	
	IC_{50}	R^2	IC_{50}	R^2
10	9.86 μM	0.9871	11.86 μM	0.9086
11	13.46 μM	0.9489	14.76 μM	0.9454
11a	350 nM	0.9046	350 nM	0.9200
11b	233 nM	0.9526	233 nM	0.9085
AZA*	462 nM	0.9656	389 nM	0.9500

Note: AZA acetazolamide, hCA-I and II human carbonic anhydrase isoenzymes I and II.
*AZA used as a standard inhibitor for hCA-I and hCA-II isoenzymes.

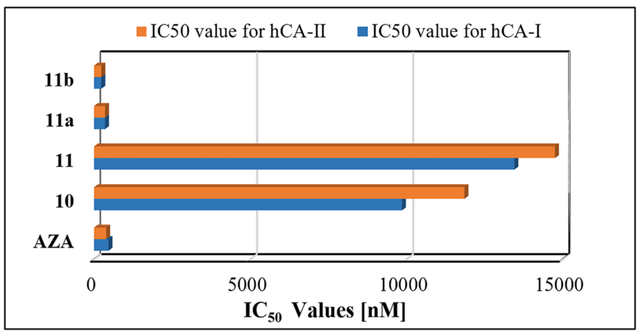

FIGURE 13 Comparison plot of IC_{50} values of **10**, **11**, **11a**, **11b** molecules for hCA-I and hCA-II

that the experimental IC_{50} values and the binding constant obtained by docking results are in good agreement.

The hCA-I active site was defined as the catalytic Zn (II) ion located at the bottom of a cone-shaped cavity active site surrounded by THR199, PHE91, LEU131,

TABLE 6 Binding energies of the best conformers for each reg.ion, Boltzmann-averaged binding energies (ΔG_{ba}) and ΔG_{ba} dependent binding constants (K_b)

	Compounds	Reg 1	Reg 2	Reg 3	Reg 4	Reg 5	ΔG_{ba} (kcal mol^{-1})	K_b ($\times 10^7$)
hCA-I (5GMM)	**ZnPc**	−12.2	−11.8	−11.7	−11.3	−11.7	−11.88	51.1
	CoPc	−12.5	−12.1	−12.1	−10.8	−11.3	−12.20	87.8
	10	−7.1	−6.6	−6.1	−6.0	−4.8	−6.75	8.95×10^{-3}
	11	−9.6	−8.5	−7.6	−7.2	−6.2	−9.36	0.725
	Pox	−8.6	−7.5	−7.5	−7.3	−7.2	−8.19	0.101
	Aza	−6.4	−6.1	−5.4	−5.2	−4.5	−6.09	2.93×10^{-3}
hCA-II (3 M98)	**ZnPc**	−12.0	−10.7	−10.3	−10.3	−10.4	−11.66	35.0
	CoPc	−13.5	−10.8	−8.6	−8.3	−9.9	−13.46	739.0
	10	−7.2	−7.2	−5.8	−6.3	−6.2	−6.99	0.0134
	11	−8.8	−8.6	−7.2	−6.8	−7.5	−8.56	0.188
	Pox	−7.5	−7.2	−6.7	−6.8	−6.3	−7.17	0.018
	Aza	−6.5	−5.5	−5.1	−4.7	−5.3	−6.12	3.04×10^{-3}

Note: The binding regions of hCA-I were surrounded by Reg1: HIS119/GLN92/THR199, Reg2:GLN242/HIS243/TYR7, Reg3: LYS113/ASN245/THR100, Reg4: ASN24/GLN249/GLU14, Reg5: LYS34/LEU251/ASP32 residues. The binding regions of hCA-II were surrounded by Reg1: PRO201/GLN92/GLU236, Reg2: PHE131/HIS64/LEU198, Reg3: LYS127/GLN137/THR208, Reg4: LYS225/PHE179/SER166, Reg5: LYS113/HIS15/PRO250 residues.

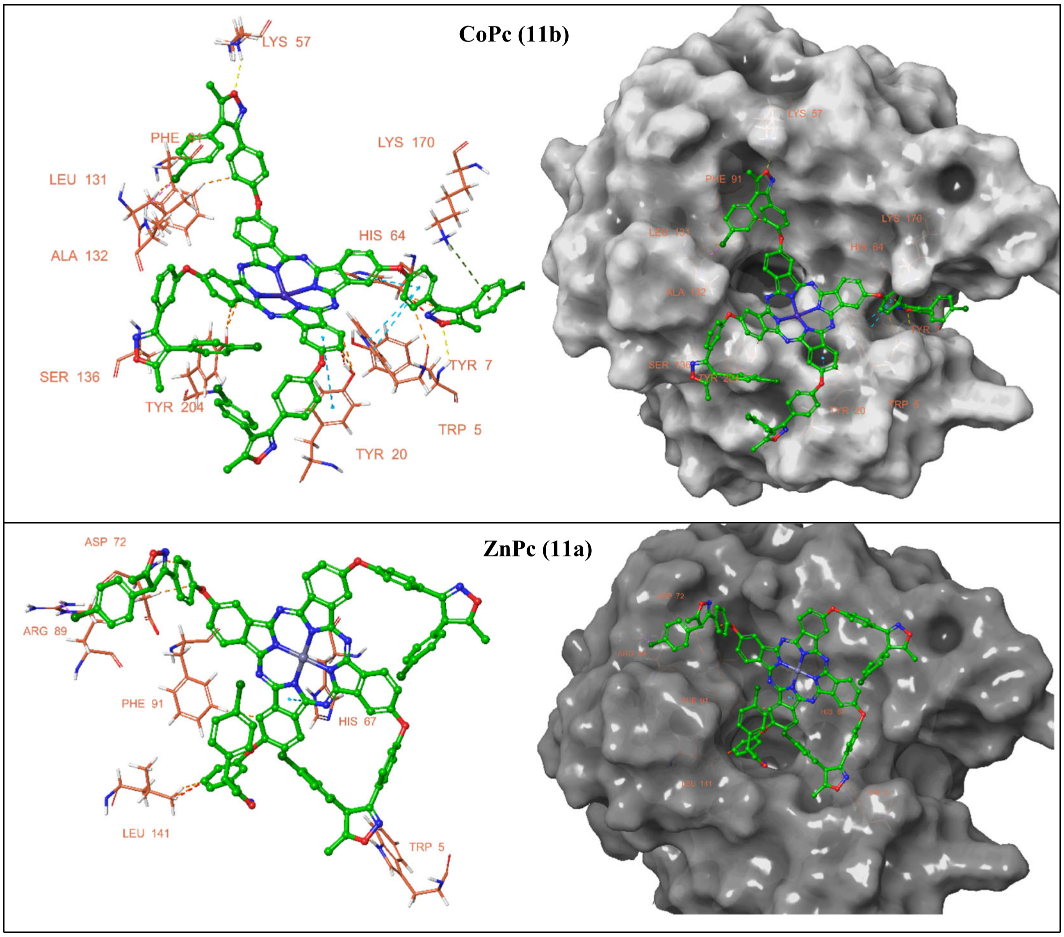

FIGURE 14 The docking pose of the Pc complexes on the binding region of hCA-I. Yellow dashed line: H-bond, light blue dashed line: Pi-Pi stacking, green dashed line: Pi-cation, orange dashed line: Hydrophobic interactions

LEU141, LEU198, HIS64, HIS67, and HIS200. In this study, region 1 (Reg1) was selected as the top of a cone-shaped cavity active site.[61] Likewise, the hCA-II cavity active site was surrounded by THR198, PRO201, LEU203, VAL134, ILE91, VAL121, PHE130, and LEU140 amino acid residues.[62] Both Pc complexes were located at the canonical entrance of the active region of the hCA-I and hCA-II enzymes, while free ligands and reference molecules extended toward the active catalytic site of the enzymes. The binding modes of CoPc and ZnPc were demonstrated in Figures 14 and 15.

The molecular structures of both Pc complexes are very similar. Since the difference of metal atoms in the center of the molecule affects the partial charge distribution on the molecule, it causes a change in the interaction forces as well as the differentiation of the interacted amino acids.[96] The binding interactions of Pc complexes were given in Table 7.

When the interactions between hCA-I and CoPc were examined, the oxygen atom of the peripheral ligand formed a hydrogen bond with the NH of TRP7 and LYS57 residues with distances 2.72 and 2.42 Å, respectively. The chlorine atom formed the halogen bond with ALA132 at 2.72 Å length. The aromatic rings of CoPc also form a pi-pi interaction with the aromatic ring of TRP5, TYR20, and HIS64 and pi-cation interaction with the LYS170 amino acid residue. The Co atom of the Pc complex is exactly placed as a cover over the entrance to the cone-shaped active site, as it appears on the electrostatic surface of the enzyme. It also settles strongly in this region by forming hydrophobic interactions with amino acids such as HIS64, PHE91 and ALA132. Closing the gate of the active site in this way is thought to cause inhibition by preventing the substrate from reaching the catalytic Zn (II) ion at the bottom of this region.

Unlike CoPc, in ZnPc, one of the peripheral groups extends toward the active site with interacting with LEU141 and HIS67 active site residues and closes the entrance to this region, while the rest of the molecule is settled on the surface by making strong interactions like hydrogen bonding, halogen bond, pi-pi interaction and hydrophobic interactions. In interactions of ZnPc with hCA-I, the oxygen atoms formed H-bonds with TRP5

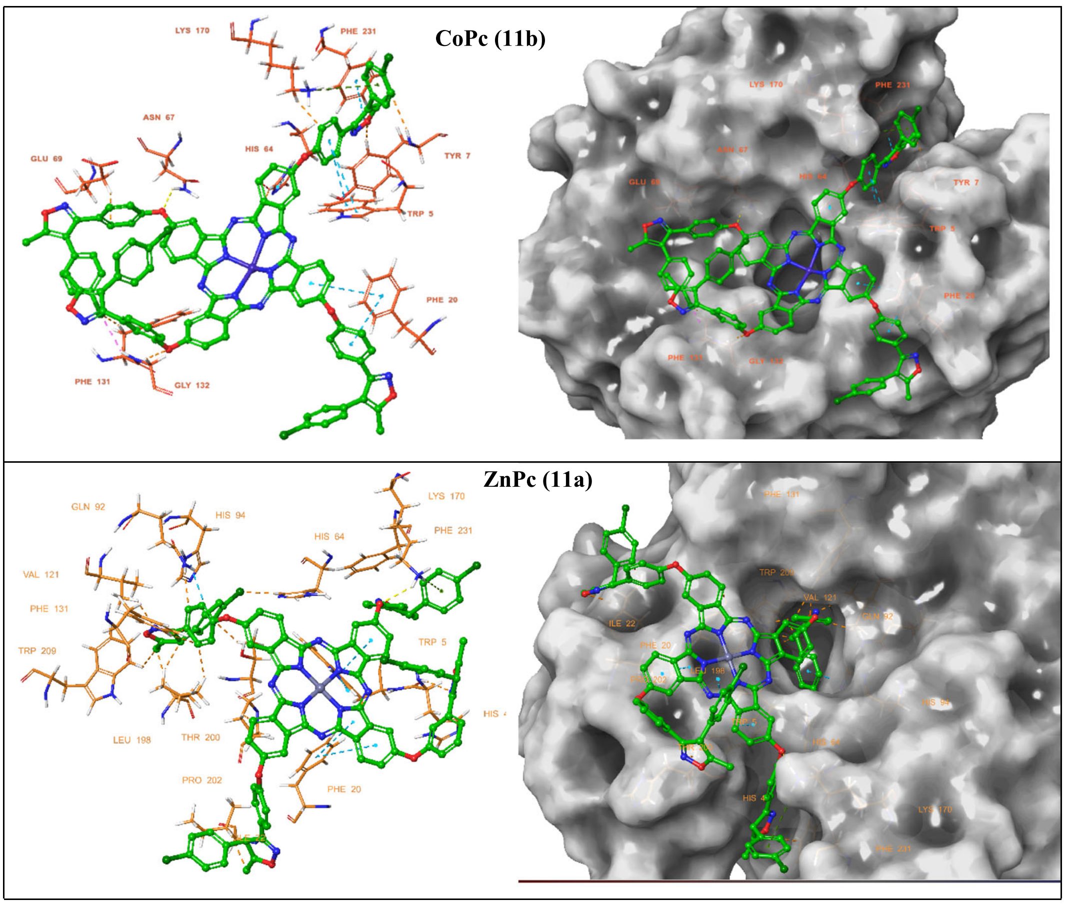

FIGURE 15 The docking pose of the Pc complexes on the binding region of hCA-II. Yellow dashed line: H-bond, light blue dashed line: Pi-Pi stacking, green dashed line: Pi-cation, orange dashed line: polar interactions

TABLE 7 The binding interactions of Pc complexes with hCA-I and hCA-II. The bond lengths were given as the bracket for hydrogen and halogen bond in Angstrom

	Compounds	Hydrogen Bonds (Å) * Halogen Bonds (Å)	π-Stacking *π-Cation	Hydrophobic Interactions
hCA-I	CoPc	TRP7(2.72), LYS57(2.42), ALA132(2.74) *	TRP5, TYR20, HIS64, LYS170*	HIS64, PHE91, ALA132
	ZnPc	TRP5(2.29), ASP72 (2.80), ARG89(2.87) *	TRP5, HIS67	TYR20, ILE60, VAL62, PHE91, LEU131, LEU141, LEU198, PRO202
hCA-II	CoPc	TYR7(2.72), ASN67(2.32), GLY132(2.38) *	TRP5, PHE231, PHE20, HIS64, LYS170*	GLY6, GLU69, GLN92, PHE131, PRO202, LEU204
	ZnPc	LYS170(2.25), TYR7(2.34)	TRP5, PHE20	GLN92, ILE22, HIS64, LEU198, PRO202, LEU204, PHE231

(2.29 Å) and ASP72 (2.80 Å). Chlorine atom was performed halogen bond with ARG89 (2.87 Å).

When the interaction of hCA-II and metallophthalocyanine is examined, similar interactions with hCA-I and a similar location to the enzyme binding site were observed. While the CoPc metallic central active zone was located in the form of a cap on the cone-shaped active site, one of the side groups in ZnPc attempts to move toward the active zone, causing the metallic catalytic zone to be inactivated. CoPc makes hydrogen bonding with the enzyme through amino acids TYR7 (2.72 Å) and ASN67 (2.32 Å), and halogen bond through GLY132 (2.38 Å). Pi-pi stacking and pi-cation interactions occur through the amino acid residues TRP5, PHE231, PHE20, HIS64, and LYS170. GLU69, ILE91, PHE131, PRO202, and LEU204 amino acids contribute to the binding energy through hydrophobic interactions. In ZnPc, between the metal complex and hCA-II enzyme, H-bond with LYS170, TYR7, pi-pi interactions with TRP5, PHE20 and hydrophobic interactions with GLN92, ILE22, HIS64, LEU198, PRO202, LEU204, and PHE231 were also observed.

4 | CONCLUSION

In this study two new and novelty metallophthalocyanines bearing selective oxygenase inhibitor derivatives based azole ring were designed synthesized, characterized, chemical, physical characters were conducted. For the synthesis, compound **9** was prepared from the compound **7** and **8** according to the known method firstly. Follow up the dehydrogenation of compound **9**, using H_2/Pd in absolute methanol as in literature with slightly modification was afforded selective COX inhibitor derivative **10** in quantitative yield. For modification of new and novelty metallophthalocyanines, the COX inhibitor derivative **10** was reacted with 4-nitro-phthalonitrile to afforded compound **11** in quantitative yield. Phthalonitrile **11** was well documented construction for phthalocyanine ring. Thus, compound **11** was reacted with Zn $(OAc)_2.2H_2O$ and Co $(OAc)_2.4H_2O$ respectively in DMF using (2–3) drop DBU at reflux temperature, produced compound **11a** in 48% yield (ZnPc) and **11b** in 63% yield (CoPc) after isolation and purification. The inhibitory activity of COX-inhibitor based metallophthalocyanines **11a**, **11b** and azole bearing ligand **10**, **11** on hCA-I and hCA-II izoenzymes were tested, and the inhibition test results were compared with acetazolamide under the same conditions. In addition, experimental inhibition results were supported using molecular docking simulation. The binding affinities interactions of these new complexes were found to be better than the reference drug molecules acetazolamide and polmacoxib.

ACKNOWLEDGMENTS

This work was financially supported by Scientific and Technological Research Council of Turkey (TÜBITAK) (Project no: 115Z446 and 217Z043). This study was carried out at Sakarya University Organic Chemistry Laboratory.

AUTHOR CONTRIBUTIONS

Emel Karakılıç: Validation; visualization. **Zuhal alım:** Data curation; formal analysis; validation. **Mustafa Emirik:** Software; validation.

CONFLICT OF INTEREST

The authors declare that there is no conflict of interest.

DATA AVAILABILITY STATEMENT

The data that support the findings of this study are available in the supporting information of this article.

ORCID

Emel Karakılıç https://orcid.org/0000-0002-8447-2851
Zuhal Alım https://orcid.org/0000-0003-1977-1756
Mustafa Emirik https://orcid.org/0000-0001-9489-9093
Arif Baran https://orcid.org/0000-0002-4117-5099

REFERENCES

[1] H. S. Majumdar, A. Bandyopadhyay, A. J. Pal, *Org. Electr.* **2003**, *4*, 39.
[2] M. S. Ağırtaş, *Dyes Pigm.* **2007**, *74*, 490.
[3] M. S. Ağırtaş, B. Cabir, S. Özdemir, *Dyes Pigm.* **2013**, *96*, 152.
[4] S. Darwish, I. K. E. Zawawi, A. S. Riad, *Thin Solid Films* **2005**, *485*, 182.
[5] Z. R. Hong, Z. H. Huang, X. T. Zeng, *Thin Solid Films* **2007**, *515*, 3019.
[6] Y. Liu, Q. Ren, Z. Su, B. Chu, W. Li, S. Wu, F. Jin, B. Zhao, X. Ya, J. Wan, D. Fan, F. Zhang, *Org. Electronics.* **2012**, *13*, 2156.
[7] J. Y. Kim, A. J. Bard, *Chem. Phy. Letters.* **2004**, *383*, 11.
[8] G. Williams, S. Sutty, R. Klenkler, H. Aziz, *Solar Cells.* **2014**, *124*, 217.
[9] L. Giribabua, V. K. Singh, T. Jella, Y. Soujanya, A. Amat, F. De Angelis, A. Yella, P. Gao, M. K. Nazeeruddin, *Dyes Pigm.* **2013**, *98*, 518.
[10] V. K. Singha, P. Salvatori, A. Amat, S. Agrawal, F. De Angelis, M. K. Nazeeruddin, N. V. Krishna, L. Giribabu, *Inorg. Chim. Acta* **2013**, *407*, 289.
[11] K. C. Lin, T. Doane, L. Wang, P. Li, S. Pejic, M. E. Kenney, C. Burda, *Solar Cells.* **2014**, *126*, 155.
[12] T. Asahi, H. Y. Yoshikawa, M. Yashiro, H. Masuhara, *App. Surf. Sci.* **2002**, *197-198*, 777.
[13] D. D. Erbahar, I. Gürol, G. Gümüş, E. Musluoğlu, Z. Z. Öztürk, V. Ahsen, M. Harbeck, *Sens. Actuators, B* **2012**, *173*, 562.
[14] L. Valli, *Adv. Colloid. Inter. Sci.* **2005**, *116*, 13.
[15] P. Fit, M. Vrnata, D. Kopecky, J. Vlcek, J. Skodova, J. Bulir, M. Novotny, P. Pokorny, *Appl. Surf. Sci.* **2014**, *302*, 37.
[16] J. H. Shu, H. C. Wikle, B. A. Chin, *Sens. Actuators, B* **2010**, *148*, 498.
[17] Y. Zhang, X. Chen, M. Guo, S. Zhang, Z. Jiang, *Mat. Letters.* **2008**, *62*, 3453.
[18] S. J. Mathews, S. C. Kumar, L. Giribabu, S. V. Rao, *Optics Commun.* **2007**, *280*, 206.
[19] A. Günsel, M. Kandaz, F. Yakuphanoglu, W. A. Farooq, *Synt. Metals.* **2011**, *161*, 1477.
[20] A. S. Komolov, P. J. Møller, *Synt. Metals.* **2003**, *138*, 119.
[21] A. Sun, G. Zhang, Y. Xu, *Mater. Letters.* **2005**, *59*, 4016.
[22] H. D. Diesbach, E. V. D. Weid, *Helv. Chim. Acta* **1927**, *10*, 886.
[23] A. G. Dandridge, H. A. E. Drescher, J. Thomas, *Dyes British. Patent* **1929**, *No*, 322169.
[24] P. Agostinis, E. Buytaert, H. Breyssens, N. Hendrickx, *Photochem. Photobiol. Sci.* **2004**, *3*, 721.
[25] A. Casas, G. D. Venosa, A. Batlle, *Resistance to Photodynamic Therapy in Cancer.* **2015**, *5*, 29.
[26] E. Güzel, G. Y. Atmaca, A. Erdoğmuş, M. B. Koçak, *J. Coord. Chem.* **2017**, *70*, 2659.
[27] E. Güzel, A. Atsay, S. Nalbantoglu, N. Şaki, A. L. Dogan, A. Gül, M. B. Koçak, *Dyes Pigm.* **2013**, *97*, 238.
[28] I. J. Macdonald, T. J. Dougherty, *J. Porphyr. Phthalocyanines.* **2001**, *5*, 105.
[29] D. Arıcan, A. Erdoğmuş, A. Koca, *Thin Solid Films* **2014**, *550*, 669.
[30] V. Francis, *Neurochem. Res.* **1980**, *5*, 1047.
[31] R. Schwarcz, T. Hökfelt, K. Fuxe, G. Jonsson, M. Goldstein, L. Terenius, *Exp. Brain Res.* **1979**, *37*, 199.
[32] S. Greene, K. Watanabe, J. Braatz-Trulson, L. Lou, *Biochem. Pharmacol.* **1995**, *50*, 861.
[33] J. K. Larsen, L. Krogh-Nielsen, K. Brøsen, *Health Care: Current Reviews.* **2016**, *4*, 1.
[34] Y. Li, F. Wang, L. Wu, M. Zhu, G. He, X. Chen, F. Sun, Q. Liu, X. Wang, W. Zhang, *Infection and Drug Resistance.* **2019**, *12*, 721.
[35] Q. Zhuang, Y. Bian, W. Wang, J. Jiang, B. Feng, T. Sun, J. Lin, M. Zhang, S. Yan, B. Shen, F. Pei, X. Wen, *BMJ Open.* **2016**, *6*, 1.
[36] S. Dadiboyena, A. Nefzi, *Eur. J. Med. Chem.* **2010**, *45*, 4697.
[37] I. Yamawaki, K. Ogawa, *Chem. Pharm. Bull.* **1988**, *36*, 3142.
[38] M. L. Pati, P. Vitale, S. Ferorelli, M. Iaselli, M. Miciaccia, A. Boccarelli, G. D. Mauro, C. G. Fortuna, T. F. S. Domingos, L. C. R. P. Silva, M. Pádula, L. M. Cabral, P. C. Sathler, A. Vacca, A. Scilimati, M. G. Perrone, *Eur. J. Med. Chem.* **2019**, *164*, 59.
[39] A. Alberola, A. M. Gonzalez, M. A. Laguna, F. J. Pulido, *J.Org. Chem.* **1984**, *49*, 3423.
[40] O. Singh, K. R. Kakularam, P. Reddanna, P. Aparay, *Protein and Peptide Lett.* **2015**, *22*, 903.
[41] R. Meleddu, S. Distinto, F. Cottiglia, R. Angius, M. Gaspari, D. Taverna, C. Melis, A. Angeli, G. Biaanco, S. Deplano, B. Fois, S. Del Prete, C. Capasso, S. Alcaro, F. Ortuso, M. Yanez, C. T. Supuran, E. Maccion, A. C. S. Med, *Chem. Lett.* **2018**, *9*, 1045.
[42] C. T. Supuran, A. Scozzafava, *Exp Opin Ther Patents* **2000**, *10*, 575.
[43] A. M. Alaa, A. Angeli, A. S. El Azab, M. E. A. Hammouda, M. A. El-Sherbeny, C. T. Supuran, *Bioorg. Chem.* **2019**, *84*, 260.
[44] H. T. Kim, H. Cha, K. Y. Hwang, *Biochem. and Biophys. Research Com.* **2016**, *478*, 1.
[45] A. Weber, A. Casini, A. Heine, D. Kuhn, C. T. Supuran, A. Scozzafava, G. Klebe, *J. Med. Chem.* **2004**, *47*, 550.
[46] A. Di Fiore, C. Pedone, K. D'Ambrosio, A. Scozzafava, G. De Simonea, C. T. Supuran, *Chem. Lett.* **2006**, *16*, 437.
[47] A. Aydin, M. Akkurt, S. Turanli, D. Lengerli, E. Banoglu, N. D. Ozcelik, *Acta Crystallographica Section E: Crystall. Comm.* **2021**, *77*(4), 346.
[48] L. Di Nunno, P. Vitale, A. Scilimati, S. Tacconelli, P. Patrignani, *J. Med. Chem.* **2004**, *47*, 4881.
[49] H. Chunlin, S. Zuming, Z. Qizhong, L. Shijun, L. Ning, H. Feihe, *J. Org. Chem.* **2008**, *73*, 5872.
[50] G. M. Sheldrick, *Acta Cryst.* **2008**, *A64*, 112.
[51] Mercury, version 3.0; CCDC, available online via http://ccdc.cam.ac.uk/products/mercury.
[52] L. J. Farrugia, *J. Apply. Cryst.* **1999**, *32*, 837.
[53] A. L. Spek, *PLATON-A Multipurpose Crystallographic Tool*, Utrecht University, Utrecht **2005**.
[54] Z. Alım, N. Kilinc, B. Sengul, S. Beydemir, *Chem. Biol. Drug Des.* **2015**, *86*, 857.
[55] Z. Alım, *J. Biochem. Mol. Toxicol.* **2018**, *32*, 22194.

[56] Z. Alım, Z. Köksal, M. Karaman, *Pharma. Reports.* **2020**, *72*, 1738.
[57] K. M. Wilbur, N. G. Anderson, *J Biol Chem.* **1948**, *176*, 147.
[58] M. M. Bradford, *Anal. Biochem.* **1976**, *72*, 248.
[59] U. K. Laemmli, *Nature* **1970**, *227*, 680.
[60] C. Turkes, M. Arslan, Y. Demir, D. Çoçajd, A. R. Nixhad, Ş. Beydemir, *Bioorg. Chem.* **2019**, *89*, 103004.
[61] H. T. Kim, H. Cha, K. Y. Hwang, *Biochem. Biophys. Res. Commun.* **2016**, *478*, 1.
[62] E. Čapkauskaitė, L. Baranauskienė, D. D. Golovenko, E. Manakova, S. Gražulis, S. Tumkevičius, D. Matulis, *Med. Chem.* **2010**, *18*, 7357.
[63] Schrödinger Release, *2018-4: Protein Preparation Wizard*, Epik, Schrödinger, LLC, New York, NY **2016** Impact, Schrödinger, LLC, New York, NY, 2016; Prime, Schrödinger, LLC, New York, NY, 2018.
[64] Schrödinger Release 2018-4, *Maestro*, Schrödinger, LLC. Published online **2018**.
[65] Y. Cao, L. Li, *Bioinformatics* **2014**, *30*, 1674.
[66] Y. Liu, M. Grimm, W. T. Dai, M. C. Hou, Z. X. Xiao, Y. Cao, *Acta Pharmacol. Sin.* **2020**, *41*, 138.
[67] G. M. Morris, D. S. Goodsell, R. S. Halliday, R. Huey, W. E. Hart, R. K. Belew, A. J. Olson, *J. Comput. Chem.* **1998**, *19*, 1639.
[68] L. Ozalp, S. Sağ Erdem, B. Yüce-Dursun, Ö. Mutlu, M. Özbil, *Comput. Biol. Chem.* **2018**, *77*, 87.
[69] V. Ngwenya, I. N. Booysen, A. Mambanda, *J. Coord. Chem.* **2019**, *72*, 1131.
[70] H. Enkelkamp, R. J. M. Nolte, J. Porphyr, *Phthalocyanines* **2000**, *4*, 454.
[71] G. Gümrükçü, G. K. Karaoğlan, A. Erdoğmuş, A. Gül, U. Avcıata, *J. Chem. Volume.* **2014**, *2014*, 1.
[72] G. Dilber, M. Durmuş, H. Kantekin, *Dyes Pigm.* **2019**, *160*, 267.
[73] Y. Zorlu, F. Dumoulin, M. Durmuş, V. Ahsen, *Tetrahedron* **2010**, *66*, 3248.
[74] A. Baran, S. Çol, E. Karakılıç, F. Özen, *Polyhedron* **2020**, *175*, 114205.
[75] T. Nyokong, V. Ahsen, *Science Business Media. New York.* **2012**, 664.
[76] A. Ogunsipe, T. Nyokong, *J. Porphyr. Phthalocyanines.* **2005**, *9*, 121.
[77] J. R. Darwent, I. McCubbin, D. Phillips, *J. Chem. Soc.* **1982**, *78*, 347.
[78] M. Idowu, T. Nyokong, *J. Photochem. Photobiol. A.* **2009**, *204*, 63.
[79] J. Rose, in *Advanced Physico-chemical Experiments*, (Ed: S. I. Pitman), London **1964** 257.
[80] H. Karaca, İ. Şişman, E. Güzel, S. Sezer, F. Selimoğlu, B. Ergezen, M. Karaca, V. Eyüpoğlu, *J. Coord. Chem.* **2018**, *71*, 1606.
[81] M. S. Liao, S. Scheiner, *J. Chem. Phys.* **2001**, *114*, 9780.
[82] N. Nombona, T. Nyokong, *Dyes Pigm.* **2009**, *80*, 130.
[83] C. C. Leznoff, A. B. P. Lever, *Phthalocyanines, Properties and Applications*, Vol. 1, VCH, New York **1989** 133.
[84] Y. Derin, R. F. Yılmaz, İ. H. Baydilek, V. E. Atalay, A. Özdemir, A. Tutar, *Inorg. Chim. Acta* **2018**, *482*, 130.
[85] B. Yılmaz, E. Güzel, N. Menges, İ. Şişman, M. K. Şener, *Solar Energy.* **2018**, *174*, 527.
[86] T. Keles, B. Barut, Z. Biyiklioglu, A. Özel, *Dyes Pigm.* **2017**, *139*, 575.
[87] M. S. Ağırtaş, B. Cabir, S. Özdemir, V. Okumuş, A. Arslantaş, *ChemistrySelect* **2017**, *2*, 11352.
[88] L. Yuan, L. Gui, Y. Wang, Q. Zhang, L. Zhou, S. Wei, *Spectrochim. Acta, Part A* **2016**, *158*, 1.
[89] G. Ayyannan, M. Mohanraj, G. Raja, N. Bhuvanesh, R. Nandhakumar, C. Jayabalakrishnan, *J Photochem Photobiol B Biol.* **2016**, *163*, 163.
[90] B. Chidananda, K. R. Venugopala Reddy, K. M. Pradeep, M. N. K. Harish, C. D. Mruthyunjayachari, S. D. Ganesh, N. S. Vijaykumar, P. Malthesh, *Der Pharma Chemica.* **2016**, *8*, 198.
[91] M. Kozarski, A. Klaus, M. Niksic, D. Jakovljevic, J. P. F. G. Helsper, L. J. L. D. V. Griensven, *Food Chem.* **2011**, *129*, 1667.
[92] G. Zengin, S. Uysal, R. Ceylan, A. Aktümsek, *Ind. Crop. Prod.* **2015**, *70*, 1.
[93] T. Arslan, Z. Biyiklioglu, M. Senturk, *RSC Adv.* **2018**, *8*, 10172.
[94] T. Arslan, N. Cakir, T. Keles, Z. Biyiklioglu, M. Senturk, *Bioorg. Chem.* **2019**, *90*, 103100.
[95] T. Tian, L. Weng, S. Wang, X. Weng, L. Zhang, X. Zhou, *J. Porphyrins Phthalocyanines* **2009**, *13*, 893.
[96] E. Güzel, Ü. M. Koçyiğit, P. Taslimi, İ. Gülçin, S. Erkan, M. Nebioğlu, B. S. Arslan, İ. Şişman, *J. Biomol. Struct. Dyn.* **2020**, 1.

SUPPORTING INFORMATION

Additional supporting information may be found in the online version of the article at the publisher's website.

How to cite this article: E. Karakılıç, Z. Alım, M. Emirik, A. Baran, *Appl Organomet Chem* **2022**, *36*(3), e6537. https://doi.org/10.1002/aoc.6537